Phys Chem Minerals
DOI 10.1007/s00269-014-0729-2

ORIGINAL PAPER

Experimental petrology of peridotites, including effects of water and carbon on melting in the Earth's upper mantle

David H. Green

Received: 8 October 2014 / Accepted: 13 December 2014

Abstract For over 50 years, the use of high-pressure piston/cylinder apparatus combined with an increasing diversity of microbeam analytical techniques has enabled the study of mantle peridotite compositions and of magmas derived by melting in the upper mantle. The experimental studies have been guided by the petrology and geochemistry of peridotites from diverse settings and by the remarkable range of mantle-derived magma types. Recent experimental study using FTIR spectroscopy to monitor water content of minerals has shown that fertile lherzolite (MORB-source upper mantle) at ~1,000 °C can store ~200 ppm H_2O in defect sites in nominally anhydrous minerals (olivine, pyroxenes, garnet and spinel). Water in excess of 200 ppm stabilizes amphibole (pargasite) at $P < 3$ GPa up to the lherzolite solidus. However, at $P > 3$ GPa, water in excess of 200 ppm appears as an aqueous vapour phase and this depresses the temperature of the upper mantle solidus. Provided the uppermost mantle (lithosphere) has $H_2O < 4{,}000$ ppm, the mantle solidus has a distinctive P, T shape. The temperature of the *vapour-undersaturated* or *dehydration solidus* is approximately constant at 1,100 °C at pressures up to ~3 GPa and then decreases sharply to ~1,010 °C. The strongly negative dT/dP of the vapour-undersaturated solidus of fertile lherzolite from 2.8 to 3 GPa provides the basis for understanding the lithosphere/asthenosphere boundary. Through upward migration of near-solidus hydrous silicate melt, the asthenosphere becomes geochemically zoned with the 'enriched' intraplate basalt source (>500 ppm H_2O) overlying the 'depleted' MORB source (~200 ppm H_2O). From the study of primitive MOR picrites, the modern mantle potential temperature for MORB petrogenesis is ~1,430 °C. The intersection of the 1,430 °C adiabat with the vapour-saturated lherzolite solidus at ~230 km suggests that upwelling beneath mid-ocean ridges begins around this depth. In *intraplate* volcanism, diapiric upwelling begins from shallower depths and lower temperatures within the asthenosphere and the upwelling lherzolite is enriched in water, carbonate and incompatible elements. Magmas including olivine melilitites, olivine nephelinites, basanites, alkali picrites and tholeiitic picrites are consequences of increasing melt fraction and decreasing pressure at melt segregation. Major element, trace element and isotopic characteristics of island chain or 'hot-spot' magmas show that they sample geochemically distinct components in the upper mantle, differing from MORB sources. There is no evidence for *higher-temperature* 'hot-spot' magmas, relative to primitive MORB, but there is evidence for higher water, CO_2 and incompatible element contents. The distinctive geochemical signatures of 'hot-spot' magmas and their 'fixed' position and long-lived activity relative to plate movement are attributed to melt components derived from melting at interfaces between old, oxidised subducted slabs (suspended beneath or within the deeper asthenosphere) and ambient, reduced mantle. In convergent margin volcanism, the inverted temperature gradients inferred for the mantle wedge above the subducting lithosphere introduce further complexity which can be explored by overlaying the phase relations of appropriate mantle and crustal lithologies. Water and carbonate derived from the subducted slab play significant roles, magmas are relatively oxidised, and distinctive primary magmas such as boninites, adakites and island arc ankaramites provide evidence for fluxing of melting in refractory harzburgite to lherzolite by slab-derived hydrous adakitic melt and by wedge-derived carbonatite.

D. H. Green (✉)
Centre for Ore Deposit and Exploration Studies, School of Earth Sciences, University of Tasmania, Hobart, TAS 7000, Australia
e-mail: david.h.green@utas.edu.au

Published online: 23 January 2015

Keywords IMA medal lecture · Upper mantle · Lithosphere/asthenosphere boundary · Basalt petrogenesis · Lherzolite

Introduction

The modern Earth is the most dynamically active of the inner, 'rocky' planets of our solar system. The global dynamic behaviour is characterised as 'Plate Tectonics'. In the Plate Tectonics paradigm, the upper mantle to depths of 600–700 km behaves in a very distinctive way. Thin lithospheric plates with little internal deformation are bounded by narrow linear plate boundaries of high deformation (spreading centres, subduction zones and transform faults). The lithospheric plates are compositionally complex with major division into continental crust, oceanic crust and lithospheric mantle. Differences in elevation (implying density and compositional differences) between continental and oceanic crust are well defined, but plate margins commonly transgress and are independent of ocean/continent boundaries, i.e. the plate margins are lithospheric mantle phenomena. The boundary between overlying lithospheric plates and underlying asthenosphere (lithosphere/asthenosphere boundary—LAB) occurs within peridotite. The crust and upper mantle are characterised by geophysical methods, and these observations must be interpreted in mineralogical and petrological terms. The singular nature of modern Earth geodynamics implies particular compositional (density) and rheological properties within the upper mantle. These properties are determined by the interplay of variation in chemical compositions, pressure (P) and temperature (T) and are studied in the subdisciplines of geochemistry, mineralogy, petrology and petrophysics. For over 50 years, the use of high-pressure piston/cylinder apparatus combined with an increasing diversity of microbeam analytical techniques has enabled experimental study of mantle peridotite compositions and of magmas derived by melting in the upper mantle. It is the purpose of this paper to summarise the petrology and petrogenesis of the upper mantle, focussed on those studies in which I and my students and collaborators have contributed. The nature of the presentations, as the IMA medal lecture at the European Mineralogical Conference in Frankfurt in August, 2012, and as the Shen-su Sun Memorial Lecture at the Chinese Annual Petrology and Geodynamics Conference in Lanzhou in September, 2012, expresses the continuity and summarises the results of an experimental, petrological and geochemical programme investigating magmas, the upper mantle and deep crust. A pervasive theme in this programme is the use of natural mantle samples (i.e. mantle-derived magmas and peridotites and basalts with high-pressure mineral parageneses), to guide the investigations and the choice of experimental compositions and conditions.

Composition of modern upper mantle: the 'pyrolite' concept

The term 'pyrolite' was coined by Ringwood (1962) for a model peridotite composition for the upper mantle dominated by olivine and orthopyroxene and derived by mixing mantle-derived magma (basalt) with harzburgite (interpreted as refractory residue after basalt extraction). The selection of a parental or primitive basalt and of the complementary harzburgite composition, and the selection of the mixing proportions, obviously determine the specific pyrolite composition. The least refractory compositions among spinel lherzolite xenoliths in intraplate basalts, and among spinel lherzolite complexes showing high-temperature decompression P, T paths, were used as guides, constraining the target composition to have 3–4 wt% CaO and Al_2O_3 and olivine of $Mg^{\#} = 89–90$. Green and Falloon (1998) detail the evolution of the pyrolite concept and the calculation of the model compositions referred to as 'Hawaiian Pyrolite' (HPY) and 'mid-ocean ridge pyrolite' (MPY) (Table 1). These two compositions differ mainly in minor element contents reflecting the difference between the choice of basaltic magma used in the 'pyrolite' calculation, i.e. parental mid-ocean ridge basalt (MORB) or ocean island basalt (OIB or 'hot-spot' basalt). A third composition is a natural spinel lherzolite, Tinaquillo lherzolite (TQ), which conforms to the CaO, Al_2O_3 and olivine $Mg^{\#}$ constraints for pyrolite but is lower in Na_2O, TiO_2 and K_2O. These model upper mantle compositions are also referred to as 'enriched' (HPY), 'fertile' (MPY) and 'depleted' (TQ)—the terms applying to relative enrichment or depletion in incompatible elements. Hart and Zindler (1986) also presented a model upper mantle composition based on arguments derived from chondritic compositions, bulk Earth models and both high-temperature orogenic lherzolites and spinel lherzolite xenoliths. This composition (HZ1) is very close to MOR Pyrolite (MPY), i.e. it is a 'fertile' lherzolite composition (see Table 1).

The inferred upper mantle composition controls the mineralogy at particular P, T conditions and thus the phases which determine the major element compositions of melts. In the context of source, melt and residue in the upper mantle, minor and trace elements may be designated as 'compatible' if they have significant solid solution ($D = c_{mineral}/c_{melt} > 0.1$; c = concentration) in the major phases (olivine, orthopyroxene, clinopyroxene, plagioclase, spinel or garnet) or 'incompatible' if $c_{mineral}/c_{melt} < 0.1$. Among the minor elements present in natural basalts and peridotites, K, P, H, C and S are highly incompatible with respect to the major phases listed previously. Na has $c_{plagioclasel}/c_{melt} \sim 1$ and $c_{clinopyroxene}/c_{melt} \sim 0.1$ at low pressure (<1.5 GPa), but $c_{clinopyroxene}/c_{melt}$ increases with pressure. Ti has low incompatibility, having significant solid

Table 1 Major element chemical compositions of model upper mantle which have been used for experimental studies (see text)

	Tinaquillo lherzolite	HZ lherzolite	MORB Pyrolite	Hawaiian Pyrolite	Harzburgite
SiO_2	44.95	46.2	44.74	45.2	46.62
TiO_2	0.08	0.18	0.17	0.71	0.08
Al_2O_3	3.22	4.08	4.37	3.54	0.65
Cr_2O_3	0.45	0.4	0.45	0.43	0.57
FeO	7.66	7.59	7.55	8.47	4.91
MgO	40.03	37.96	38.57	37.5	46.19
CaO	2.99	3.23	3.38	3.08	0.73
Na_2O	0.18	0.33	0.4	0.57	0.05
K_2O	0.02	0.03	0	0.123	0.03
P_2O_5	0.01	0.02	0	0.04	0
NiO	0.26	0.28	0.26	0.2	0
$Mg^{\#}$	90.01	89.9	90.1	89	94.4

solution in spinel, clinopyroxene and garnet. Some trace elements have solid solutions with $c_{mineral}/c_{melt} > 0.1$, such as Sr in plagioclase or HREE in garnet, and are widely used as indicators for roles of particular minerals in melting or crystal fractionation processes. The highly incompatible elements are extremely important in magma genesis as they form additional phases even at low concentrations in the mantle and thus introduce new controls on the mantle solidus. In the experimental programme summarised in this paper, H and C are shown to have dramatic effects on mantle melting and magma compositions. These elements may occur either as vapour phase (H_2, H_2O, CH_4, CO_2), as stoichiometric components in hydrous silicates (amphibole, mica), in minor or trace minerals (diamond or graphite, carbonates, apatite), dissolved in silicate or carbonatite melts, or in defects in nominally anhydrous minerals (NAMs).

None of the peridotite compositions described above is designated as 'refractory', i.e. harzburgite with olivine > enstatite ≫ chromite, and containing <~1 wt% of Al_2O_3 or CaO. Such harzburgite compositions are widely sampled in large, partially serpentinised, ultramafic bodies obducted on to continental crust at some convergent plate margins (basal units of ophiolite complexes) and among sea-floor samples (abyssal peridotites, Dick 1989; Niu 2004). Mass balance calculations using compositions of parental MOR picrite or 'hot-spot' (Hawaii) picrite and the peridotite compositions of Table 1 show that 30–35 % melting of the lherzolites is required to yield 'refractory' harzburgite residue. Also, the subduction process includes complex mixing of subducted slab and overlying mantle, including remelting fluxed by C + H + O volatiles. Subduction returns cool lithosphere, variably depleted by MOR, intraplate and convergent margin volcanism, into the upper mantle creating mantle chemical heterogeneity from 'pyrolite' to refractory harzburgite. Density differences due to $Mg^{\#}$ and the absence of garnet at high pressure, particularly in the harzburgite compositions, mean that chemical heterogeneity may drive buoyant upwelling in the upper mantle, e.g. if fertile MORB-source mantle encloses subducted harzburgite (Niu and O'Hara 2008).

Plate tectonics, the distinctive 'thin plate' behaviour of the crust and upper mantle of the Earth, is a first-order planetary characteristic. To understand the geophysics and geodynamics of the Earth, we must understand its petrology and mineralogy. The Earth's upper mantle is lherzolitic in composition, and geodynamics and magmatism in plate tectonics are constrained by the petrology of lherzolite.

Melting of pyrolite

Melting in the upper mantle (the solidus of lherzolite) has a major effect on rheology and controls magmatism, i.e. we must have the correct petrology to interpret the geophysics and model the geodynamics. In Fig. 1, the experimentally determined solidi for anhydrous and carbon-free lherzolites of depleted to enriched character are compared. The subsolidus mineralogy is olivine > orthopyroxene > clinopyroxene, with a pressure-dependent phase which is plagioclase at low pressure, spinel at intermediate pressure and garnet at higher pressure. Solidi have positive dT/dP, and differences between the solidi reflect the bulk compositions, particularly the Na/Ca (and thus the plagioclase composition at low pressure). Relative to MOR Pyrolite, the solidus for Hawaiian Pyrolite is ~50 °C lower and that for Tinaquillo lherzolite is ~25 °C higher at 1 GPa.

Several additional concepts are introduced in Fig. 1. An oceanic intraplate geotherm (conductive geotherm for the non-convecting boundary layer) is illustrated and does not intersect the solidi, particularly those of the fertile MORB Pyrolite or enriched Hawaiian (OIB) Pyrolite. Melting occurs when upwelling from the deeper convecting mantle follows approximately adiabatic decompression paths. Two examples are illustrated. One with potential

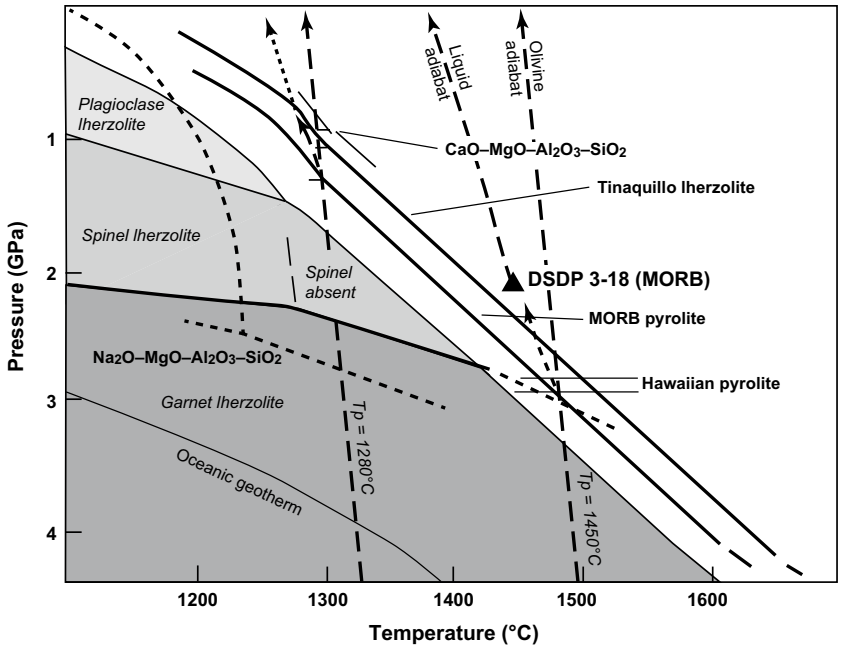

Fig. 1 Experimentally determined *dry* solidi for three compositions ('enriched', 'fertile' and 'depleted') of Table 1 and subsolidus stability fields for anhydrous mineral assemblages for 'enriched' Hawaiian Pyrolite (HPY) composition. Adiabats for mantle potential temperatures of 1,280 and 1,430 °C are shown, assuming a subsolidus gradient of 10 °C/GPa and a liquid adiabat of 30 °C/GPa. The *solid triangle symbol marks* the inferred depth (2 GPa, 1,450 °C) of magma segregation for primary MOR picrite DSDP3-18 (Green et al. 1979) (modified from Green and Falloon 2005)

temperature T_p = 1,280 °C intersects the MORB Pyrolite solidus at ~1.2 GPa, at or close to the upper pressure limit of plagioclase in the subsolidus mineralogy. As melting occurs, the latent heat of melting and increasing melt fraction deflect the *P*, *T* path from the subsolidus 'olivine adiabat', until liquid segregates and travels through dykes or dunite channels to the surface (i.e. with an upper temperature bound of the liquid adiabat). The characteristics of magmas formed in this example are determined by phase relations of the melting process of MORB Pyrolite at 0.8–1.2 GPa, 1,250–1,300 °C. Low-degree melts leave residual Ol + Opx + Cpx + Plag + Cr-spinel, and with increasing melt fraction, plagioclase and clinopyroxene are sequentially eliminated (Green and Ringwood 1967; Jaques and Green 1980; Falloon et al. 1988, 1999, 2001; Falloon and Green 1988; Chalot-Prat et al. 2010, 2013).

A second example depicts a mantle potential temperature T_p = 1,450 °C so that the anhydrous solidus is crossed at ~3 GPa, 1,480 °C, near the boundary between aluminous pyroxenes ± aluminous spinel peridotite and garnet peridotite. Melts are initially in equilibrium with residual Ol + Opx + Cpx + Al-spinel, and clinopyroxene is eliminated and spinel becomes more Cr-rich as melt fraction increases.

To apply the MORB Pyrolite anhydrous melting study to interpret the origins of natural MORB, it is necessary to identify the most primitive melt compositions among glass or olivine + glass samples. The liquidus phases of such primitive melts have been determined as a function of pressure, seeking conditions of co-saturation with [olivine($Mg^{\#}$ = 91) + orthopyroxene ± clinopyroxene ± Cr–Al spinel]. In Fig. 1, an example (DSDP 3–18 + 15 % olivine) has olivine + orthopyroxene as liquidus phases at 2 GPa, 1,430 °C (Green et al. 1979) and is compatible with ~20 % melt fraction of the MORB Pyrolite composition. At this melt fraction, subcalcic diopside is close to elimination, or is eliminated, from the residue which is olivine > enstatite > Cr–Al spinel. As residual enstatite contains 2.8 % CaO and 7 % Al_2O_3 and there may be ~1 % trapped melt, the residual lithosphere after MORB extraction contains ~1 % CaO and ~2 % Al_2O_3, i.e. it is 'residual' or 'depleted' but not 'refractory' in composition.

The role of water in the upper mantle

Figure 1 summarises the relationship between mantle upwelling, melting and melt segregation leaving residual peridotite on the assumption that the mantle and melts extracted from it at mid-ocean ridge locations, are dry. However, studies of quenched MORB glasses show that they contain 0.1–0.2 wt% H_2O, and primitive OIB may contain up to ~1 wt% H_2O. In Island Arc and Andean-type magmatism believed to be sourced from melting within the mantle wedge lying above the subducted slab, the role of high water contents is well established. Recognition of the role of water in intraplate and convergent margin magmas led to the experimental study of the effects of water on the melting behaviour of lherzolite.

In the 1970s, three experimental studies of the effects of water on the melting behaviour of mantle lherzolite (Kushiro et al. 1968; Green 1973b; Millhollen et al. 1974) found solidus temperature for water-saturated conditions to reach a minimum ~1,000 °C at 1.5–2 GPa and to have a positive

dT/dP at higher pressures. All three studies used fertile lherzolite compositions and observed that the amphibole pargasite was stable to the solidus and immediately above the solidus, to 2.5 or 3 GPa. A fourth study, by Mysen and Boettcher (1975) using several different natural peridotites and very high water/rock proportions, interpreted much lower solidus temperatures at >1 GPa, reaching a minimum of ~800 °C at ~2.5 GPa. In interpreting experimental products, there is difficulty in the identification of quenched glass as sourced from aqueous vapour or from hydrous silicate melt. Criteria based on refractive indices of glass, textures of charges and identification of Fe-enriched quench phases were used to distinguish subsolidus, vapour-bearing experiments from above-solidus, silicate melt-bearing mineral assemblage (Kushiro et al. 1968; Green 1973b; Millhollen et al. 1974; Nehru and Wyllie 1975). Green (1976) used change in mineral composition (particularly increasing $Mg^{\#}$ of all residual phases and Na and K contents of pargasite) and breakdown of pargasite to locate the water-saturated solidus. Experiments with 2 wt% H_2O in the 'Pyrolite-40 % olivine' composition (Hawaiian Pyrolite, Table 1) were also carried out to compare with the larger data set (Green 1973b) of experiments with 10 wt% H_2O (equivalent to 1.2 and 6 wt% H_2O, respectively, in the 'pyrolite' composition). Further studies to explore the effect of bulk composition on the solidus temperature and on pargasite stability were carried out by Wallace and Green (1991), Mengel and Green (1989) and Niida and Green (1999). The compositions (Table 1) were depleted lherzolite (Tinaquillo lherzolite), K-enriched lherzolite (NHD lherzolite) and fertile lherzolite (MOR Pyrolite) compositions, respectively. These experimental studies found that the vapour-saturated solidi (water-rich vapour) were the same within experimental error, but the pressure and temperature limits to pargasite stability and the temperature of the dehydration solidi were sensitively dependent on the bulk composition, particularly on the Na, K and Ti contents (also Fumagalli et al. 2009). All three studies used water contents of 1 wt% or less in experiments. Pargasite was stabilized to higher temperature and pressure by higher Na, Ti and K contents with the counter-intuitive consequence that the temperatures of the *dehydration solidi* at 1–3 GPa *increased* from the depleted Tinaquillo lherzolite to the enriched Hawaiian Pyrolite and NHD Peridotite (Wallace and Green 1991). Based on these experimental studies and the petrology of basalts and peridotites, a model for the upper mantle invoking pargasite stability in the lithosphere and melting in the asthenosphere was presented (Green and Liebermann 1976). The role of pargasite at the solidus and the complex shape of the dehydration solidus have not been recognised in most geophysical investigations or in numerical/geophysical modelling of the upper mantle and of its melting behaviour, preference being given to use of the dry solidi (Fig. 1, and syntheses of studies of melting in dry peridotitic compositions e.g. McKenzie and Bickle 1988). There appear to be several reasons for this:

1. The asthenosphere as the MORB source is perceived as 'dry' or has negligible water and carbon;
2. The effect of *P*, *T* change along the geotherm on seismic properties of minerals is sufficient to explain the seismic low velocity zone (LVZ) as a subsolidus phenomenon. Melting is not required;
3. The melt migrates rapidly even at small melt fraction and could not be retained in the asthenosphere;
4. The water contents are low in MORB-source mantle, and water is sufficiently soluble in nominally anhydrous minerals (NAMs, i.e. olivine, orthopyroxene, clinopyroxene, and spinel or garnet) so that pargasite is not stable and the solidus is lowered only by dilute solid solution effect in NAMs. This leads to numerical modelling of hydrous melting of MORB-source mantle, treating water and its effect on the solidus as a dilute trace component in NAMs.

In the earlier experimental studies, including those with water contents estimated as ~2,000–3,000 ppm H_2O (Green 1973b, 1976; Wallace and Green 1991; Mengel and Green 1989; Niida and Green 1999), dilute solution of water in mantle minerals was ignored, and it was implicitly assumed that even 100 ppm H_2O would appear as pargasite (~0.5 modal %) or as a water-rich fluid at subsolidus conditions >3 GPa. In newer work, the consideration of water in NAMs and low water contents in MORB-source mantle led to the prediction of solidus depression by increasing water content by melt/residue partitioning relations. The role of hydrous phases such as pargasite or hydrous fluid could be ignored. The emphasis on high water contents in NAMs, and theoretical modelling of the effect of water on the mantle solidus (Katz et al. 2003; Asimow et al. 2004; Hirschmann 2006) suggested the need for further experimental studies to address the issue of pargasite stability and water in NAMs (compare Figs. 2, 3).

In addition, Grove et al. (2006) and Till et al. (2012) investigated the water-saturated melting of a model mantle composition (HZ1, Table 1) which is almost identical to MOR Pyrolite, using a bulk water content of 14.5 wt% H_2O. The water-saturated solidus was interpreted to decrease to ~1,000 °C at 1 GPa and to continue with negative dT/dP, reaching a minimum ~810 °C at ~3.5 GPa and remaining at this temperature to at least 6 GPa. If correct, the result would mean that the water-saturated solidi for basalts, sediments and fertile lherzolite would be closely similar at pressures around 4–6 GPa (Grove et al. 2006, and Fig. 6 therein). Such a relationship would have considerable importance for understanding of mixed lithologies

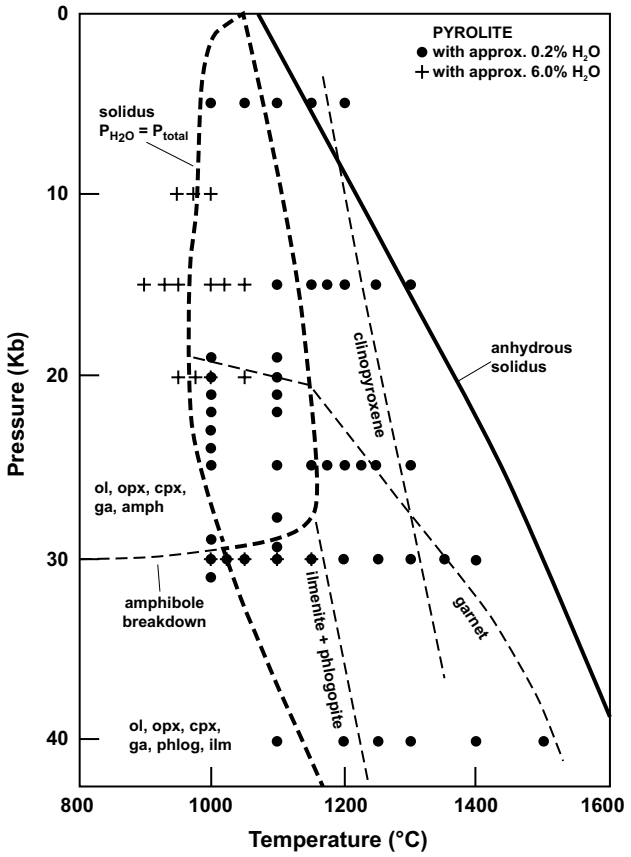

Fig. 2 Experimentally determined solidi for Hawaiian Pyrolite composition under dry conditions, with ~0.2 wt% H_2O (dehydration solidus at <3 GPa for pargasite lherzolite; vapour-saturated solidus at >3 GPa) and with ~6 wt% H_2O (vapour-saturated solidus). Phase boundaries for the disappearance of garnet, clinopyroxene, ilmenite and phlogopite above the solidus are shown for HPY + 0.2 % wt H_2O (modified from Green 1973b, 1976)

observed in ultra-high-pressure metamorphic terranes and also for hypotheses of slab/mantle wedge interactions in convergent margins. For these reasons, repetition of some of Grove et al. (2006) experiments was undertaken and led directly into an expanded study using techniques for melt and vapour traps and for Fourier transform infrared (FTIR) spectroscopic determination of water contents of NAMs as a complement to standard methods of experiment and electron microbeam study of run products (Green et al. 2010, 2011, 2014; Kovacs et al. 2012).

In this new study, a layer of lherzolite (HZ1) was placed between layers of olivine ($Mg^{\#}$ ~90) which acted as a melt trap in those experiments in which there was partial melting (Fig. 4a, b). By preparing doubly polished thick (~70 microns) sections of the experiments, the olivine layers could be analysed for water contents by FTIR spectroscopy. Experiments which were subsolidus with a water-rich vapour phase present were porous with euhedral crystals and intergranular, fragmented, extremely thin 'frothy' glass films, either in very small amounts with small bulk water contents, or abundant in experiments with 14.5 wt% H_2O, i.e. approximately 30 vol.% aqueous vapour before quenching (Fig. 4c, d). Experiments with 14.5 wt% H_2O matching those of Grove et al. (2006) reproduced their observations, particularly the absence of pargasite at 2.5 GPa and the refractory nature of the clinopyroxene, approaching diopside with <0.2 wt% Na_2O. However, by varying the water/lherzolite proportions at 2.5 GPa, 1,000 °C (Fig. 5), it was shown that pargasite was stable at bulk water contents from ~100 to 5 wt% H_2O. Clinopyroxene showed decreasing Na_2O contents from 'dry' (2.2 wt% Na_2O, 14 modal % clinopyroxene) to 14.5 wt% H_2O (<0.2 wt% Na_2O). Pargasite also showed decreasing Na_2O and K_2O from 'dry' (3.7 wt% Na_2O, 0.8 % K_2O; 4 modal % pargasite) to 2.9 wt% H_2O (3.2 wt% Na_2O, 0.4 wt% K_2O). Pargasite was unstable with 7.25 and 14.5 wt% H_2O. Experiments at 2.5 GPa and higher temperatures with 0.3 and 1.45 wt% H_2O added defined the vapour-saturated solidus, and experiments with 0.05 wt% H_2O, coupled with data from Niida and Green (1999) on MORB Pyrolite composition (Table 1), defined the vapour-absent field and the dehydration solidus at 2.5 GPa, 1,100 °C (Fig. 5).

The observations re-established the vapour-saturated lherzolite solidus at 2.5 GPa at ~1,010 °C, consistent with earlier studies (Kushiro et al. 1968; Green 1973b, 1976; Millhollen et al. 1974; Nehru and Wyllie 1975; Wallace and Green 1991; Mengel and Green 1989; Niida and Green 1999) and also confirmed the stability of pargasite at 2.5 GPa with low water contents. The relationships between bulk water contents, the compositions of both pyroxene and pargasite and the relative abundance of glass from vapour-phase quench show that the water-rich vapour phase leaches K_2O, Na_2O, SiO_2 and other oxides from the minerals (Figs. 4c, d, 5, 6). The water-rich vapour phase is a fluid in which the activity of H_2O is <1. However, the 'wet melting' behaviour of the model mantle lherzolite at 2.5 GPa is clearly 'normal' rather than 'supercritical', in that a solidus is clearly defined and there is a large compositional gap between a water-rich vapour with dilute solution of oxides including Na_2O, K_2O and SiO_2 and a hydrous silicate melt with ~25 wt% H_2O in solution. The interpretations (Grove et al. 2006; Till et al. 2012) that pargasite was unstable at the vapour-saturated lherzolite solidus at >2 GPa and is replaced by chlorite and that hydrous silicate melts formed in fertile lherzolite at temperatures ~820 °C from 2.5 GPa to at least 6 GPa, were shown to be incorrect (Green et al. 2014).

Based on the results at 2.5 GPa and the demonstration of the usefulness of the olivine layers as melt traps, experiments were carried out at 4 GPa and 6 GPa, using 0.145, 0.3 and 1.45 wt% H_2O. The first appearance of hydrous silicate melt was at ~1,225 °C at 4 GPa and ~1,375 °C at 6 GPa (Fig. 7). At >3 GPa, the vapour-saturated (water-rich

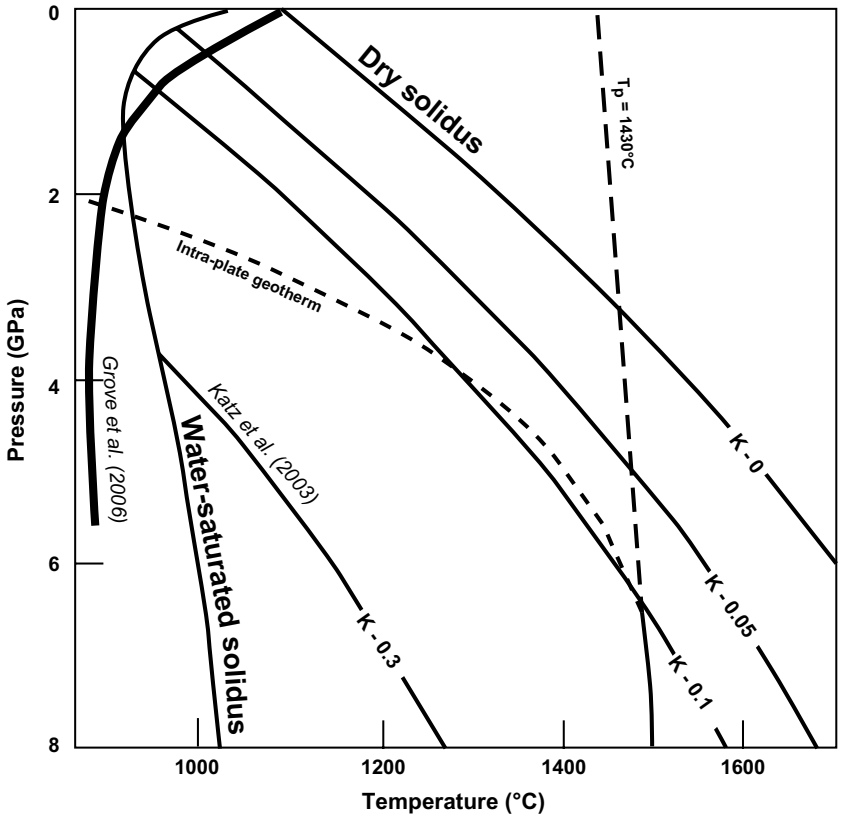

Fig. 3 Calculated solidi for mantle lherzolite as a function of bulk water content (dry, 500, 1,000, 3,000 ppm) assuming that melting is controlled by solution of water in NAMs and not by hydrous minerals or excess vapour (from Katz et al. 2003). A model intraplate geotherm and an adiabat for $T_p = 1{,}430$ °C are shown

vapour) solidus for fertile lherzolite is closely parallel to the dry solidus but lowered by ~300 °C. In the experimental study, carbon could not be entirely excluded from the experimental charge so that dolomitic carbonatite melt was present below the hydrous silicate melt solidus. At pressures below 3 GPa, the stability of pargasite at the vapour-saturated solidus and the distinctive form of the vapour-undersaturated solidus (pargasite-dehydration solidus) were confirmed (Fig. 7). The compositions of near-solidus melts are all olivine-rich and strongly silica-undersaturated, i.e. strongly nepheline-normative in petrological terms. They range from carbonate-bearing olivine melilitite at ~1 % melt fraction to olivine-rich basanite at 3–5 % melt fraction. At a given pressure, melt fraction increases with both bulk water content and temperature. With increasing pressure, the melts at the solidus decrease in Na/Ca as Na_2O becomes more compatible in clinopyroxene/melt partitioning.

In addition to the redetermination of the solidus and the mineral assemblages near the solidus, the monomineralic mineral layers above and below the lherzolite layer enabled the use of FTIR spectroscopy to measure the water contents of nominally anhydrous olivine, orthopyroxene and clinopyroxene (Kovacs et al. 2012). The data obtained are summarised in Table 2. The full data set shows very little change in water contents in NAMs across the solidus (implying very little change in water activity from aqueous fluid to water-rich melt). The experimental study demonstrated the limited solubility of water in olivine and pyroxenes (NAMs) under upper mantle conditions and the dominant role for pargasite in the water storage capacity of lherzolite in the lithosphere (Fig. 7; Table 2).

In the preceding summary of anhydrous and hydrous melting of the upper mantle, emphasis is placed on the use of complex natural compositions. The study of simple chemical systems of 1, 2 or 3 components can reveal important information, e.g. melting in the systems nepheline + forsterite + silica or kalsilite + forsterite + silica (see below); or solubility mechanisms of $(OH)^-$ in olivine with periclase (silica-undersaturated) or with enstatite (silica-saturated); or the roles of TiO_2 (stabilising the Ti-clinohumite component in olivine (Berry et al. 2005). However, the complexity of mineral solid solutions and the uncertainties in calculating activities of components (particularly H_2O) in melt, vapour or supercritical fluid mean that extrapolations from simple system studies must be checked against observations based on experiments matching as closely as possible to the compositions (including fO_2), pressures and temperatures of the Earth. The corollary to this approach is close attention to the geochemistry, petrology and geological settings of both peridotites and putative mantle-derived magmas, in order to link experiments to real Earth observations.

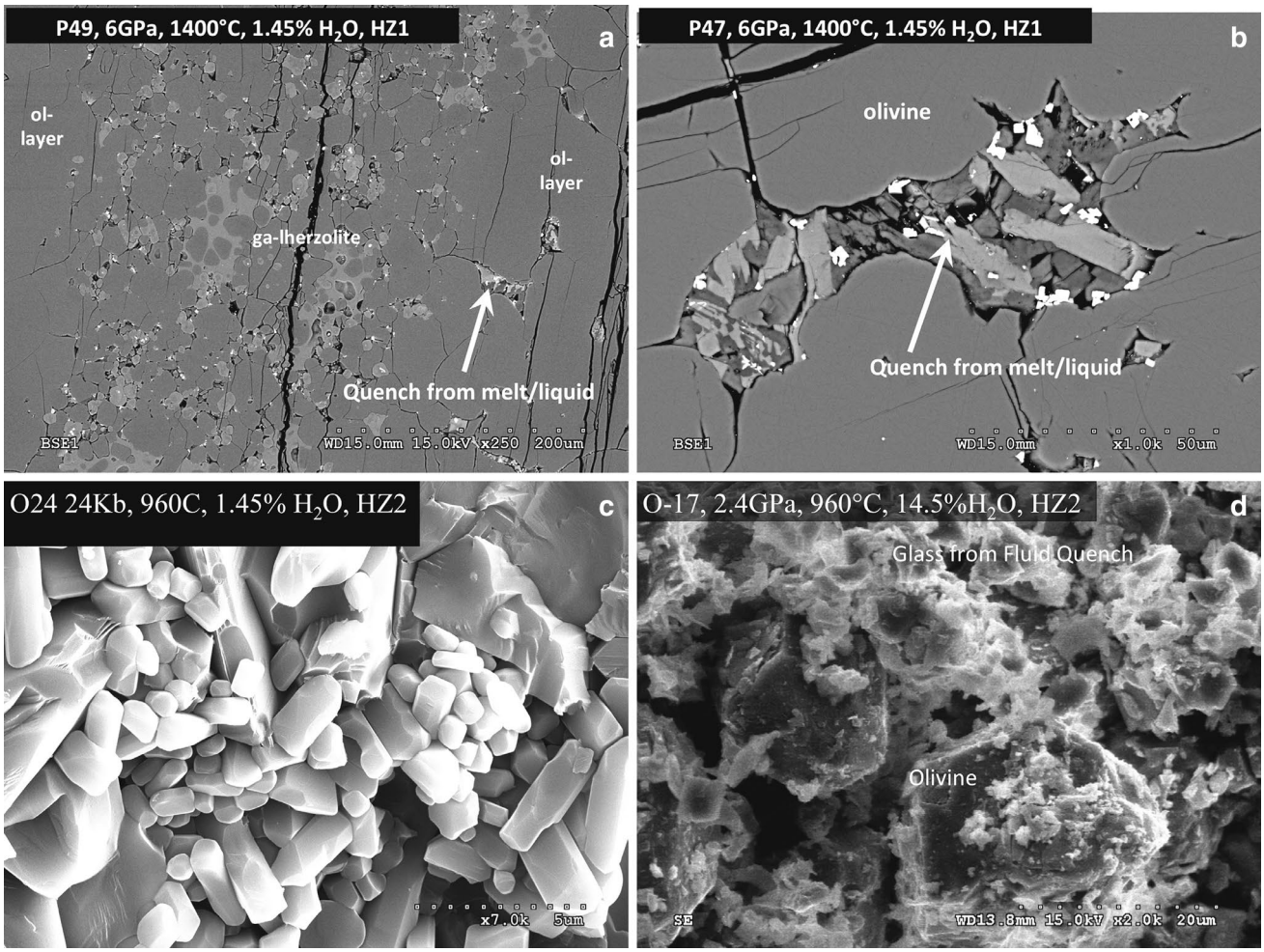

Fig. 4 SEM images illustrating experiments above and below the hydrous silicate melt solidus (from Green et al. 2014). **a** P49, HZ1 at 6 GPa, 1,400 °C, 1.45 wt% H_2O. *Image* shows the three layers of the experimental charge. The upper olivine layer (*right*) contains quenched hydrous, carbonate-bearing silicate melt in intersertal texture between olivine crystals. The middle layer is garnet lherzolite and the lower layer (*left*) is olivine with very little trapped melt. The *image* illustrates the role of the olivine layer as a melt trap for melt generated in the lherzolite layer. The olivine layer is designed for FTIR analyses (Kovacs et al. 2012). **b** P47, HZ1 at 6 GPa, 1,400 °C, 1.45 wt% H_2O. A higher-magnification image of the olivine layer shows the quenched hydrous, carbonate-bearing silicate melt in intersertal texture between olivine crystals. The quench phases include Fe-rich amphibole or clinopyroxene, dolomitic carbonate and titanomagnetite. There is also Fe-enrichment of olivine rims enclosing the melt intersert. **c** O24, HZ2 at 2.4 GPa, 960 °C, 1.45 wt% H_2O. Secondary electron image of broken surfaces of pargasite garnet lherzolite. Euhedral phases separated by pores (vapour phase) with uncommon small glass filaments. This experiment contained ~3 vol.% water-rich vapour before quenching—compare with **d**. **d** O17, HZ2 at 2.4 GPa, 960 °C, 14.5 wt% H_2O. Secondary electron image of broken surfaces of garnet lherzolite. Fragmented films of glass attached to euhedral olivine crystals and to capsule wall—interpreted as vapour-phase quench. In this experiment, the experimental charge contained ~30 vol.% water-rich vapour before quenching

The role of carbon in the upper mantle

Early experimental studies of carbon in the upper mantle addressed the stability of diamond and graphite, found in kimberlite pipes and more recently in exhumed ultra-high pressure metamorphic terranes. A parallel approach (Wyllie 1978, 1979; Wyllie et al. 1983) investigated the origin of natural intrusive and extrusive carbonatite magmas and identified an important role for carbonation reactions (olivine + CO_2 → magnesite + enstatite; olivine + diopside + CO_2 → dolomite + enstatite) in limiting the stability of CO_2-rich fluids to low pressures. Thus, dolomite is a subsolidus phase at pressures >1.5–2 GPa along mantle geotherms provided that fO_2 is sufficiently high (i.e. fO_2 ~FMQ or IW + 3–4 log units). Experimental study of the HPY composition with a small added dolomite or magnesite showed sharp depression of the solidus at ~2 GPa (Figs. 8, 10d). The vapour-saturated solidus (CO_2 vapour) is close to the dry solidus (C, H-absent) at <1.8 GPa implying low CO_2 solubility in near-solidus silicate

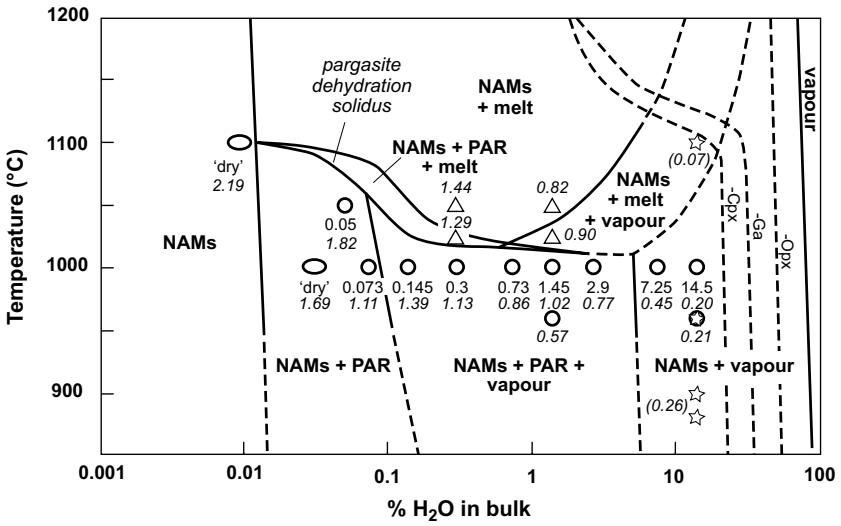

Fig. 5 Diagram at ~2.5 GPa expressing phase stability as a function of water content (note logarithmic scale) and temperature, based on the experimental results on HZ lherzolite compositions (Green et al. 2014) and prior studies, particularly Niida and Green (1999) and Grove et al. (2006). The experiments in which a water-rich silicate melt was observed in HZ composition are shown by a triangle, those with a water-rich vapour (porous and with fluid inclusions or vapour phase quench) are shown by a circle, and 'dry' experiments (no added water) are shown by an ellipse. Numbers below data points at 1,000 °C are added water contents of experimental runs and *numbers* in *italics* are Na_2O contents of clinopyroxenes (Fig. 6). *Asterisk symbols* and attached Na_2O contents (*bracketed*) are from Grove et al. (2006)

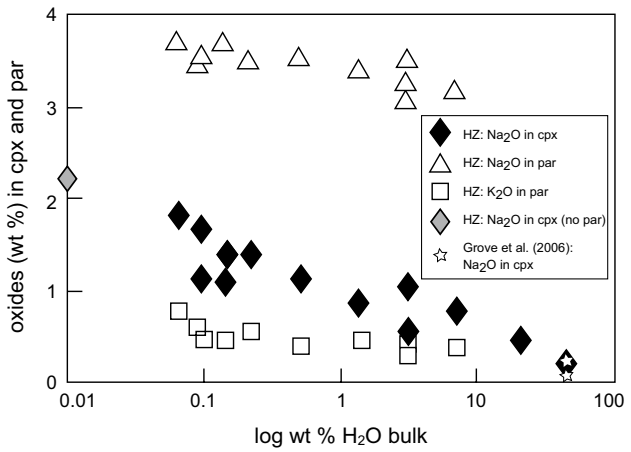

Fig. 6 Compositional variation in pargasite and clinopyroxene from subsolidus experiments at 2.4 to 2.5 GPa, 960 to 1,100 °C in either HZ lherzolite compositions, plotted against added water content (note logarithmic scale). The figure demonstrates the absence of pargasite at high water content correlating with diminishing Na_2O content in clinopyroxene. Note that, at 2.5 GPa, vapour is absent at <0.1 wt% H_2O approximately in HZ compositions (from Green et al. 2014)

melts but at pressure >2 GPa the solidus of dry dolomite-bearing lherzolite is vapour-absent and lies at temperatures slightly higher than the water-saturated solidus (Fig. 10a, d; compare Figs. 2, 7, 8).

To link the studies of HPY + H_2O with the studies of the melt-fluxing role of carbonate, experiments were carried out on HPY with very small water contents (0.3 %) and small added carbonate (Figs. 9, 10c) (Wallace and Green 1988). A further study of HPY with approximately 2 % H_2O and 2 % CO_2 yields fluid (H_2O + CO_2) excess conditions over the pressure range to 4 GPa (Fig. 10b). In this study, at low pressure where carbonates are not stable, the fluid composition is ~2:1 (H_2O/CO_2 molar) (Falloon and Green 1990). However, subsolidus dolomite is present at pressures >2 GPa, and fluids have very high H_2O/CO_2 and dissolve increasing amounts of other oxide components as pressure increases.

In these experimental studies examining the effects of H_2O and CO_2 on the melting of the enriched lherzolite HPY composition, the sample capsule was surrounded by magnesite and internally, carbon remained as carbonate or CO_2. However, in the Earth, occurrence of graphite and diamond, and evidence and arguments for decreasing fO_2 with increasing depth in the mantle, require the study of the melting behaviour of lherzolite + (C–H–O) at lower fO_2. By using graphite sample containers and an fO_2 buffer of WC–WO (tungsten carbide + tungsten oxide), which is close to fO_2 = (IW + 1 log unit), the melting behaviour of lherzolite HPY with (CH_4 + H_2O) fluid was investigated (Taylor and Green 1988) (Fig. 10e).

The experimental studies of the enriched lherzolite composition (HPY: model OIB or intraplate basalt source) with minor H_2O and CO_2 are compared in Fig. 10. The fO_2 of the upper mantle plays a key role in stabilising CO_2,

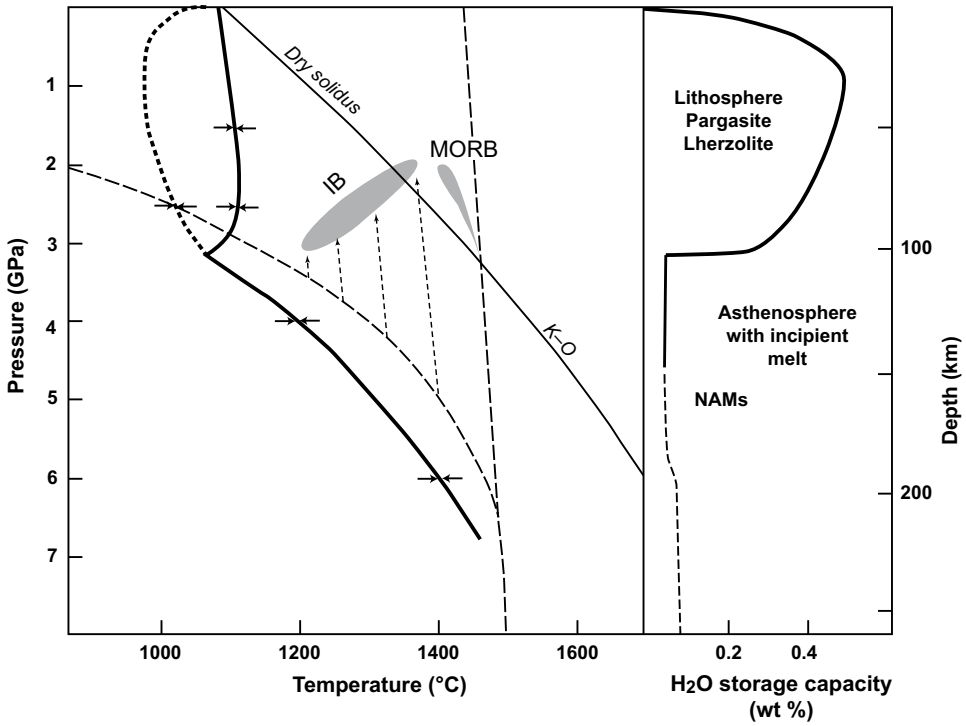

Fig. 7 Panel at *right plots* the water storage capacity of fertile, MORB-source mantle (i.e. MPY or HZ lherzolite) as a function of depth, along the vapour-saturated solidus. At <100 km approximately, pargasite is stable to the solidus, but the modal abundance of pargasite reaches a maximum at 1–1.5 GPa and decreases towards higher pressure (Niida and Green 1999)—hence, the water storage capacity decreases with modal pargasite. Pargasite becomes unstable at >3 GPa, and water storage capacity drops to that (200 ppm) which can be retained in NAMs in fertile lherzolite. Panel at *left* shows experimentally determined solidi, together with a model intraplate geotherm and mantle adiabat (T_p = 1,430 °C). The intraplate geotherm intersects the mantle dehydration solidus (pargasite-bearing lherzolite) at ~90 km and at deeper levels a small melt fraction is present if water contents are >200 ppm—providing an explanation for the asthenosphere and lithosphere/asthenosphere boundary. The geotherm is shown joining the mantle adiabat at 200–250 km, and the depth interval from 90 to 250 km is one in which a very small near-solidus melt may migrate along the geotherm, enriching the upper asthenosphere and depleting the lower asthenosphere in incompatible elements. MORB are shown as sourced from upwelling lower asthenosphere, i.e. source lherzolite with ~200 ppm H_2O, and depleted LREE and LILE element patterns, with melt fraction increasing rapidly above the anhydrous solidus and melt segregation at ~15–20 % melting at ~2 GPa. Intraplate basalts (IB), including OIB, are shown as formed by upwelling of enriched lherzolite from the geotherm through middle and upper asthenosphere. Thus, *source* water and incompatible element contents *increase* with decreasing depth and temperature of upwelling. Intraplate magmas range from olivine melilitites and nephelinites at deeper levels and smaller melt fraction, to olivine tholeiites with higher melt fraction and higher temperatures (see text; Green et al. 2014; Green and Falloon 1998, 2005)

Table 2 Water contents in nominally anhydrous minerals at the water-saturated solidus of HZ lherzolite

2.5 Gpa	
Olivine	45 ppm
Orthopyroxene	295 ppm
Clinopyroxene	980 ppm
4.0 Gpa	
Olivine	65 ppm
Orthopyroxene	310 ppm
Clinopyroxene	910 ppm
Pargasite 2.5 Gpa	~1.5 % (15,000 ppm)
Melt at 2.5 GPa	~25 %
Melt at 4.0 Gpa	~30 %

Values rounded from Kovacs et al. (2012)

dolomite or carbonatitic melt or the alternative of graphite/diamond + water-rich vapour. With little buffering capacity in either the CCO or FMQ oxygen buffers due to the very small carbon or Fe_2O_3 contents of natural mantle samples or primitive basalts, it is predictable that mantle oxidation state is variable and redox reactions occur, e.g. diamond dissolution or growth, redox melting and degassing of C–O–H fluid (Foley 2011). If model geotherms are superimposed on Fig. 10a–e, then predictions of whether melting will occur, and the nature of the melt (carbonatite or carbonate-bearing, hydrous silicate melt) are strongly dependent on the fO_2 assumed and on whether it changes with depth. If mantle fO_2 ~ (IW + 3, 4 log units) ~ FMQ, then Fig. 10b, c applies and an oceanic intraplate geotherm crosses the dolomite + garnet lherzolite field and

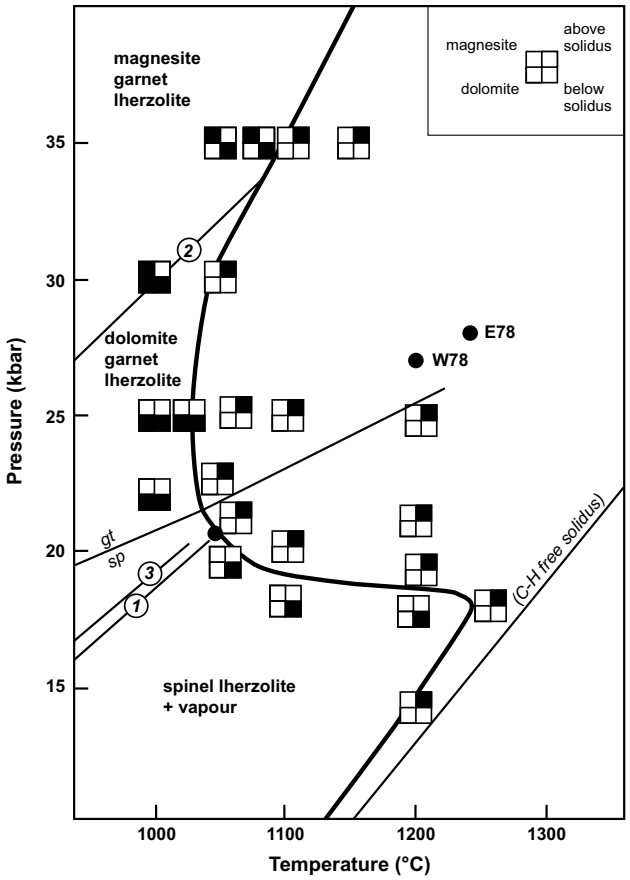

Fig. 8 Melting of enriched pyrolite (HPY) + CO_2. At low pressure (2 GPa), CO_2 is present as vapour with low solubility in silicate melts. At higher pressure (greater than the carbonation reactions to form dolomite), the melt at the solidus is sodic, dolomitic carbonatite (Falloon and Green 1989)

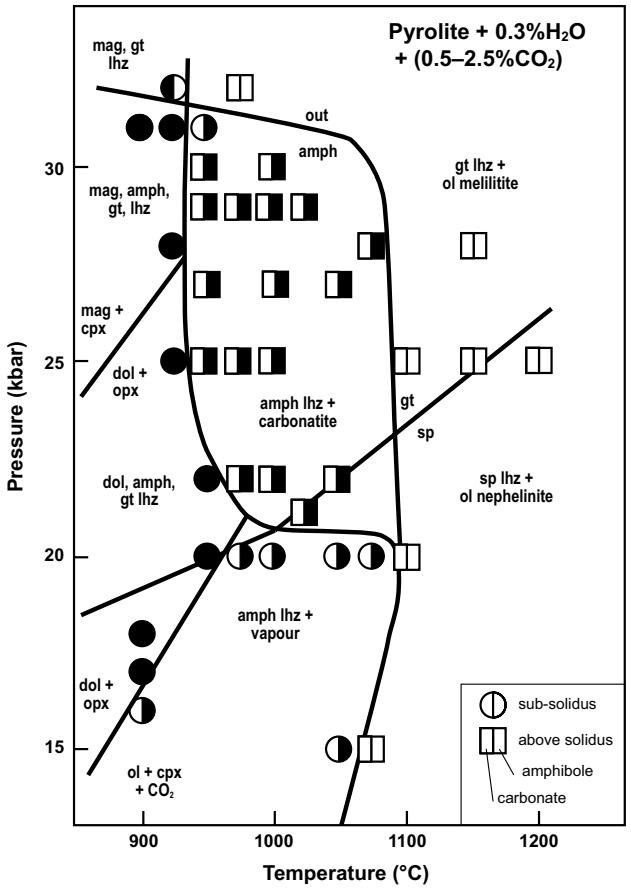

Fig. 9 Experimental melting of enriched lherzolite (HPY) with low H_2O and CO_2 contents (Wallace and Green 1988). At low pressure (<2 GPa), a CO_2-rich vapour phase is present and has little effect on the solidus which is very close to the dehydration solidus for HPY (refer Figure 2). The subsolidus mineralogy is pargasite + spinel lherzolite, and the melt formed at the solidus is a hydrous silicate melt. The carbonation reaction Ol + Cpx + CO_2 → Dol + Opx is intersected with increasing pressure (e.g. at ~1.65 GPa at 900 °C), and garnet replaces aluminous spinel at slightly higher pressure. At 2 GPa, the solidus drops abruptly to ~930 °C at 2.5–3 GPa and the melt formed at the solidus is sodic dolomitic carbonatite in equilibrium with pargasite + garnet lherzolite. Pargasite is unstable at >3 GPa, and the carbonatite melt may be accompanied by a water-rich vapour phase, but with increasing temperature the carbonatite melt dissolves increasing silica and water. Melts at temperatures above the pargasite breakdown are transitional from carbonatites to carbonate-rich olivine melilitites to olivine nephelinites

intersects the carbonatite melt solidus at ~930 °C. If mantle fO_2 ~ (IW + 2–3 log units), then carbonate is not stable and C–H–O fluid coexisting with graphite is H_2O-rich so that the relevant solidi are as illustrated in Fig. 10a (i.e. the water-saturated solidus and the dehydration solidus). There is no *P*, *T* field for carbonatite melt at this oxygen activity, but the near-solidus hydrous silicate melts contain dissolved carbonate. The intraplate geotherm crosses the solidus and enters the incipient melt field with carbonate-bearing, hydrous silicate melt at ~3 GPa, ~1,100 °C. If the Earth's mantle becomes increasingly reduced at depths greater than 150 km, then the subsolidus fluid in equilibrium with graphite- or diamond-bearing lherzolite will increase in methane/water ratio and the solidus will increase in temperature to approach the 'dry' solidus (Fig. 10e). It is clear that small quantities of water and carbon (CO_2, carbonate, graphite or diamond) have a major effect on the location of the solidus and a model of oxygen fugacity variation in the mantle is required. Before addressing this, it is helpful to consider the effects of variation of fO_2 on the compositions of melts at or near the solidus as the highly incompatible nature of carbon and hydrogen mean that these minor components will also have a major effect on melt compositions. This is illustrated by studies of several simple systems which combine forsterite (olivine) and enstatite (orthopyroxene) as refractory phases and a fusible component, either nepheline (Na) or kalsilite (K). These compositions are also linked by relative silica saturation, i.e. a parameter known to be important among natural mantle-derived magmas.

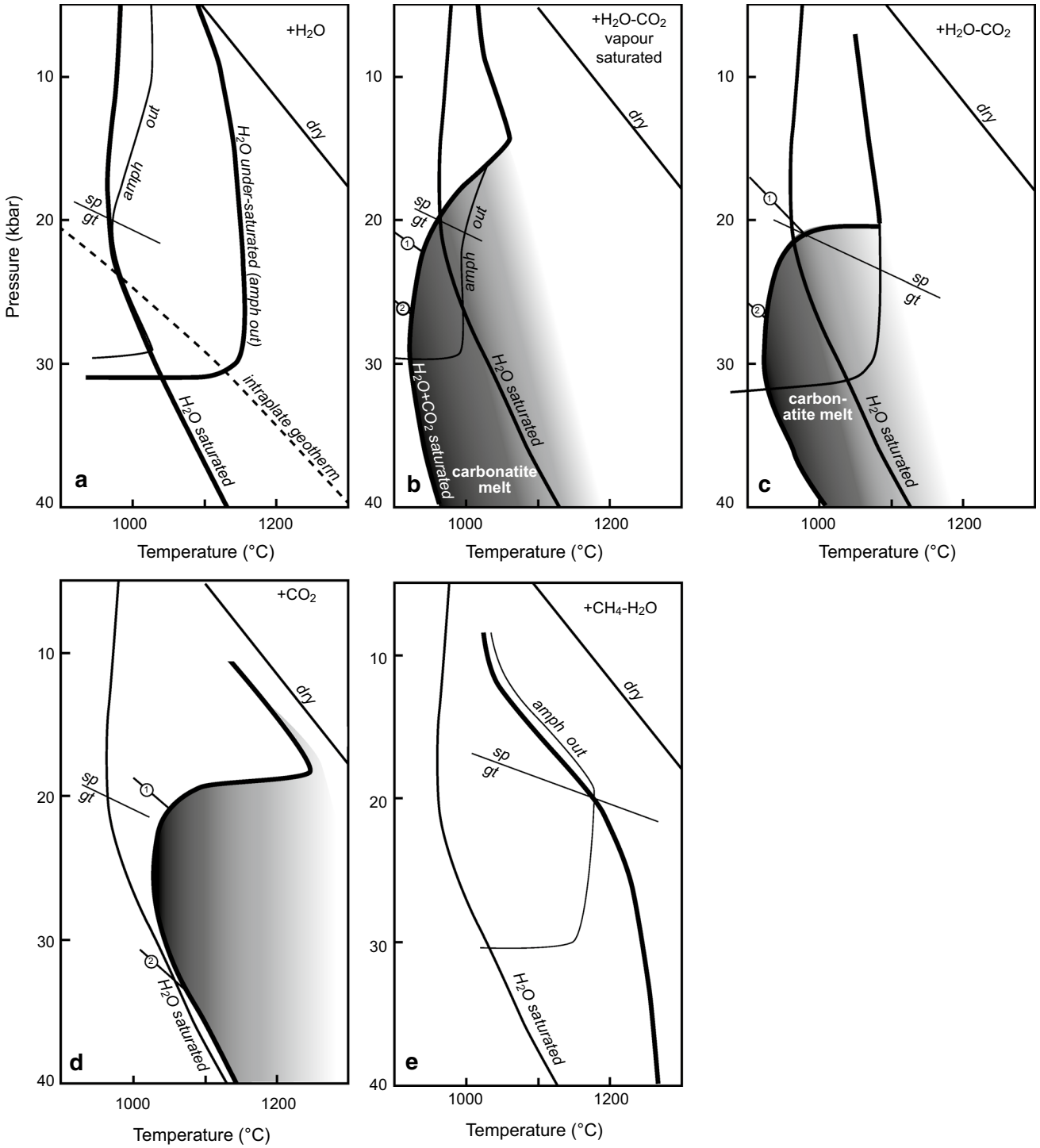

Simple system analogues for mantle melting: C, H, O effects

As noted previously, studies of simple 2–4 component chemical systems as functions of temperature and pressure are helpful in demonstrating particular reactions which contribute to relationships in the complex natural compositions. Such studies are the foundation of quantitative experimental petrology, particularly prior to the advent of microbeam techniques for analysis of experimental products in natural, multi-component compositions. They continue to be instructive in illustrating particular effects. The systems $NaAlSiO_4 + Mg_2SiO_4 + SiO_2$ (nepheline + forsterite + silica) and $KAlSiO_4 + Mg_2SiO_4 + SiO_2$ (kalsilite + forsterite + silica) contain liquidus fields for olivine and orthopyroxene, the major phases of the upper mantle.

◀ **Fig. 10** Comparison of experimentally determined solidi for enriched lherzolite (HPY) with different C, H, O species. 'Dry' and 'water-saturated' solidi are plotted in **a** to **e** for reference. Boundary for spinel to garnet lherzolite is shown, and reactions marked (1) and (2) are Ol + Cpx + CO_2 → Dol + Opx and Dol + Opx → Mag + Cpx, respectively. **a** Three solidi are illustrated: dry (C, H-absent); with H_2O < 3,000 ppm approximately (water undersaturated); with H_2O > 4,000 ppm approximately (water-saturated). See also Fig. 2 and Green (1973b). **b** Solidus for vapour-saturated conditions with 2.1 wt% H_2O and 2.0 wt% CO_2. The vapour is CO_2-rich at <1.7 GPa approximately but becomes more H_2O-rich with increasing pressure. The field for carbonatite melt is shown (*darker shading*), transitional through carbonate-rich hydrous silicate melts (*lighter shading*) to hydrous silicate melts with low carbonate content (*blank*) (Falloon and Green 1990). **c** Solidus for vapour-undersaturated conditions (2–3.2 GPa) with 0.3 wt% H_2O and 0.5–2.5 wt% CO_2. A CO_2-rich vapour is present at <2 GPa with pargasite + spinel lherzolite. Vapour is absent at or below the solidus from 2 to 3.2 GPa with H_2O and CO_2 in pargasite and carbonate (dolomite or magnesite), respectively. Water-rich vapour is present below the solidus at >3.2 GPa but dissolves in the melt with increasing temperature, as the melt transitions from near-solidus carbonatite to carbonate-bearing hydrous silicate melt. The field for carbonatite melt is shown (*darker shading*), transitional through carbonate-rich hydrous silicate melts (*lighter shading*) to hydrous silicate melts with low carbonate content (*blank*) (Wallace and Green 1988). **d** Solidus for minor carbonate content (~5 wt% dolomite or 2.4 wt% CO_2). The solidus shows sharp depression at pressure greater than the carbonation reaction and the melt at >2 GPa is dolomitic carbonatite. The solidus is at higher temperatures than the water-saturated solidus, at least to 3.5 GPa. With increasing temperature, the melt is transitional through carbonate-rich hydrous silicate melts (*lighter shading*) to silicate melts with low carbonate content (*blank*) (Falloon and Green 1989). **e** Solidus for HPY composition with C–H–O fluid buffered by tungsten carbide/tungsten oxide buffer which is approximately 1 log unit above the iron/wustite buffer fO_2 ~ (IW + 1 log unit). The fluid is (CH_4 + H_2O) and proportions vary with *P*, *T*. At *P* < 2 GPa, pargasite is stable to the solidus which lies between the dehydration solidus and water-saturated solidi (**a**). At *P* > 2 GPa, pargasite breaks down below the solidus which is then vapour-saturated for (CH_4 + H_2O) fluid (Taylor and Green 1988)

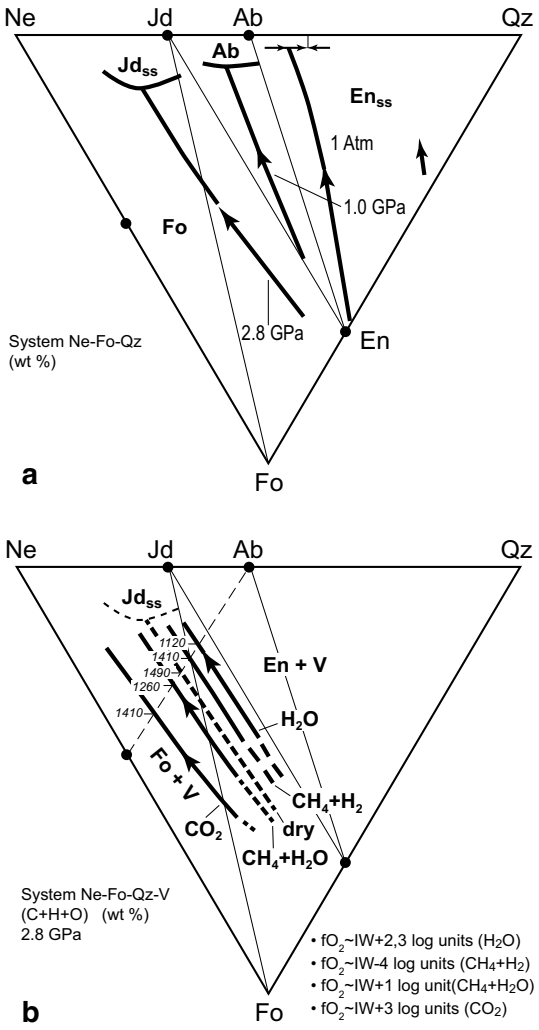

Fig. 11 **a** Liquidus fields in the system nepheline–forsterite–quartz at 1 Atmosphere, 1 and 2.8 GPa (wt%). **b** System nepheline–forsterite–quartz at 2.8 GPa with C, H, O vapour at different oxygen fugacities. The boundary (cotectic) between enstatite and forsterite as liquidus phases was located by experiments on compositions lying on the join (Albite to Ne_{55}–Fo_{45}) (Taylor and Green 1987, 1989). The positions of the cotectic with different vapour components are shown relative to the C, H-absent cotectic (**a**) with temperatures of the intersections indicated

The beginning of melting of a simple albite-bearing harzburgite occurs at the albite (Ab) + forsterite (Fo) + enstatite (Ens) invariant point, at low pressure (Fig. 11a). For olivine-rich and orthopyroxene-bearing compositions (peridotites), increase of temperature produces liquids lying on the Fo + Ens cotectic until Ens is eliminated, and higher-temperature liquids then lie on an olivine-control line to the bulk composition. The melt composition at the solidus is silica-oversaturated or 'Qz-normative' and melts remain oversaturated along the Fo + Ens peritectic, with enstatite melting incongruently Ens + Ab → Fo + $(SiO_2)_{melt}$. The effect of increasing pressure from atmospheric pressure to 3 GPa moves the invariant point to lower Qz and higher Fo contents, and albite is replaced by jadeite as the aluminous phase at the solidus. By 1 Gpa, melts at the solidus from a 'peridotite' source are silica-undersaturated (Ne-normative) and with higher temperature and melt fraction become silica-saturated (Fo + Ens normative) with both Fo and Ens melting congruently. By 2.8 GPa, jadeite is stable in the subsolidus 'peridotite', and the invariant point is strongly Ne-normative, melting is again incongruent, and the melting reaction is Fo + Jd → Ens + $(Ne)_{melt}$. Higher-temperature melts on the Fo + Ens surface remain Ne-normative up to very Fo-rich compositions.

Substituting K_2O for Na_2O in the simplified mantle analogue illustrates both similarities and differences from Ne + Fo + Qz system. At low pressure, liquids at the solidus of sanidine-bearing harzburgite are silica-oversaturated and remain so up to pressures between 1.5 and 2 GPa (Conceição and Green 2000). At 2.8 GPa, melting of sanidine-bearing harzburgite begins at ~1,460 °C, i.e. approximately

100 °C above the sodic equivalent system. The melt composition at the sanidine + forsterite + enstatite invariant point (peritectic) in Ks + Fo + Qz is silica-undersaturated but much less so than in the Ne + Fo + Qz system (Gupta and Green 1988). To summarise, increasing pressure in both the analogue peridotite compositions decreases the silica content in partial melts, and this effect is much stronger in sodic, relative to potassic, melts. Near-solidus melts are rich in Na_2O or K_2O, respectively, but become much richer in olivine with increasing melt fraction.

The effects of water and carbon on melting in these analogue systems have also been studied experimentally. Referring to Fig. 11a, b, the intersection of the Fo + Ens + melt cotectic with a compositional join, such as (Ab–$Fo_{45}Ne_{55}$), is an indicator of the position of the olivine + orthopyroxene cotectic, i.e. of the degree of silica undersaturation of the melt ('basalt') (Fig. 11b) in equilibrium with harzburgite residue. To demonstrate the effects of water and carbon on melting at the upper mantle pressures and the significance of fO_2 in controlling speciation in the C, H, O vapour phase, compositions along the join (Ab–$Fo_{45}Ne_{55}$) were studied under controlled fO_2 conditions and melt and vapour compositions determined by electron microprobe and gas chromatography/mass spectrometry (GCMS). At 2.8 GPa, melting of jadeite-bearing harzburgite begins at 1,365 °C in the absence of water or carbon. With increasing temperature, liquids lie on the Fo + Ens + melt peritectic and this crosses the (Ab–$Fo_{45}Ne_{55}$) join at 1,490 °C (Gupta et al. 1987). The melt composition is strongly nepheline-normative, i.e. it lies in the Ne–Jd–Fo field. In the presence of excess water, the field of olivine expands at the expense of enstatite and melting begins at much lower temperature. Melts along the Fo + Ens cotectic cross the (Ab–$Fo_{45}Ne_{55}$) join at 1,120 °C, and this melt is more silica-rich and less nepheline-normative than that under dry melting conditions. In the presence of CO_2, i.e. at high fO_2 and dry conditions, the Fo + Ens + melt peritectic is displaced towards the Fo + Ne join and crosses the (Ab–$Fo_{45}Ne_{55}$) join at 1,410 °C. The melt composition is extremely nepheline- and olivine-rich, approaching 'olivine nephelinite'. These experiments illustrate the opposing effects of H_2O and CO_2—although both lower the melting temperatures under oxidising conditions, H_2O moves melts towards more silica-saturated compositions whereas CO_2 drives melts to more olivine- and nepheline-normative compositions. [It should also be noted that, for CO_2 particularly, the actual depression of the *liquidus* temperature for a chosen melt (such as at 1,410 °C) is >80 °C as, in the absence of CO_2, this anhydrous composition is below its anhydrous liquidus temperature and lies in the Fo + Liq field at 1,490 °C. The example illustrates that in complex systems, liquidus depression of a particular partial melt composition by solution of water or CO_2 is not the same as depression of the solidus of the complex system].

In the Ks + Fo + Qz system, the effects of H_2O and CO_2 saturation also displace the Fo + Ens + melt peritectic in opposite directions in terms of silica saturation. However, there is an important difference in the role of water in the potassic system in that phlogopite is stable at the water-saturated solidus at high pressure and also creates conditions for vapour-undersaturated melting (dehydration melting) at lower water contents (Gupta and Green 1988). At 2.8 GPa, melting of phlogopite-bearing harzburgite begins at ~1,160 °C and melts are silica-saturated (i.e. lie in the Sa + Fo + Ens field) in contrast to the nepheline-normative compositions in the Ne + Fo + Qz system.

As carbon can be present as carbonate, CO_2, graphite or diamond, or as CH_4, it is necessary to consider the role of fO_2. In the absence of variable valence in Fe, Ti or Cr in the simple system, the effects of external buffering at different fO_2 are expressed in different C, H, O behaviour. At extremely reducing conditions using aluminium carbide + aluminium hydroxide to generate CH_4-rich fluid (estimated fO_2 ~ IW-3, 4 log units; Taylor and Green 1987), the Fo + Ens +melt peritectic boundary crosses the (Ab–$Fo_{45}Ne_{55}$) join at ~1,410 °C at a composition between the dry and water-saturated boundaries. FTIR spectroscopy demonstrated small dissolved (OH) and carbon contents (Taylor and Green 1987; Green et al. 1987) even at these extremely reducing conditions. Later experiments used graphite capsules and tungsten carbide–tungsten oxide (WC–WO) external buffer to generate carbon-saturated $CH_4 + H_2O$ fluid at fO_2 ~ IW + 1 log unit (Taylor and Green 1988). Experiments on the (Ab–$Fo_{45}Ne_{55}$) join in the Ne + Fo + Qz system showed that for these conditions at 2.8 GPa the Fo + Ens +melt peritectic boundary intersects the (Ab–$Fo_{45}Ne_{55}$) join at 1,260 °C. The intersection is slightly displaced towards lower silica saturation from the dry intersection at 1,490 °C. FTIR spectroscopy shows $(OH)^-$ and $(CO_3)^=$ absorption bands and analysis of the fluid (capsule piercing and GCMS analysis) obtained approximately 1:4 molar ratio of methane to water in the vapour phase (Taylor and Green 1988). This study shows that in the peridotite analogue, albite-bearing harzburgite, a methane + water fluid in equilibrium with graphite at 2.8 GPa and fO_2 ~ IW + 1 log unit caused depression of the liquidus of a melt coexisting with olivine and orthopyroxene by 230 °C by dissolved $(OH)^-$ and $(CO_3)^=$ and with little change in melt composition (calculated water- and CO_2-free).

The same effect was demonstrated by Odling et al. (1997) for the Hawaiian Pyrolite composition and reduced (C, O, H, S) fluid at fO_2 ~ IW + 1 log unit. At 2 GPa, 1,175 °C the melt dissolved approximately 7 % H_2O and 1.3 % CO_2. It is picritic in composition with ~16 % MgO and is hypersthene-normative. The melt comprises ~21 modal % of the Hawaiian Pyrolite composition and leaves residual olivine (44 modal %), orthopyroxene (27 %), clinopyroxene (7 %) and sulphide (1 %). The melt and residue compositions are

closely similar to the melt and residue compositions found in anhydrous melting of the Hawaiian Pyrolite composition at 2 GPa, 1,450 °C. Odling et al. (1997) note that at fO_2 ~ IW + 1 log unit and in equilibrium with graphite, melting is fluxed by carbon and hydrogen, lowering equivalent degrees of melting by ~250 °C, relative to anhydrous melting, and with little change in melt composition. At these low fO_2 conditions (which are appropriate to MORB and OIB sources), dissolved carbon as carbonate and dissolved water have opposite but roughly balancing effects on melt composition, i.e., dissolved carbonate (equivalent to only 1–2 wt% CO_2) shifts the Ol + Opx cotectic to more olivine-rich and more silica-undersaturated compositions, but this is reversed by solution of $(OH)^-$ (equivalent to ~7 wt% H_2O). Odling et al. (1997) also note that *carbon-free*, *water-saturated* melting of the Hawaiian Pyrolite composition at 2 GPa, 1,100 °C yielded a similar melt fraction, but the melt has 10.6 % MgO and has much lower normative olivine (Green 1976).

The study of simple system analogues of mantle melting shows that Na_2O enrichment and K_2O enrichment in mantle source compositions have significantly different effects on melts produced in the pressure range to 3 GPa with sodic melts being more silica-undersaturated. Importantly, solution of both water and CO_2 strongly modify melt compositions in equilibrium with olivine and enstatite at pressures above 1 GPa. The effects are opposite as solution of CO_2 drives melts to lower silica contents, and higher olivine and normative nepheline contents. Solution of water drives melts towards higher silica contents. The role of fO_2 is extremely important in stabilising carbonate or graphite at higher fO_2 and in controlling the fluid composition ($CH_4 + H_2O > H_2$) at lower fO_2 in the presence of graphite or diamond. Most importantly, at mantle fO_2 ~ IW + 1 log unit at 2.5–3.5 GPa, carbonate is not stable and, assuming carbon and/or water exceeds the storage capacity of crystalline phases, then fluid in equilibrium with graphite is dominantly ($CH_4 + H_2O$) but causes depression of solidus by >200 °C and near-solidus melts contain dissolved $(OH)^-$ and $(CO_3)^=$. The simple system Ne–Fo–Qz is a useful analogue for demonstrating the fluxing effects of both water and carbonate in depressing the solidus at pressures greater than the carbonation reactions. A most important result is the demonstration in both the analogue system and in the Hawaiian Pyrolite composition that carbon and hydrogen have significant solubility in melts at fO_2 ~ IW + 1 log unit, and flux melting when the subsolidus fluid is approaching pure water or water + methane, in equilibrium with graphite or diamond. Melts produced at these fO_2 conditions at 2–3 GPa have essentially all iron as FeO but carbon dissolved as $(CO_3)^=$. Also melt compositions (calculated water- and carbonate-free) are very similar to anhydrous and carbonate-free melts at a given melt fraction but are at ~200–250 °C lower temperature.

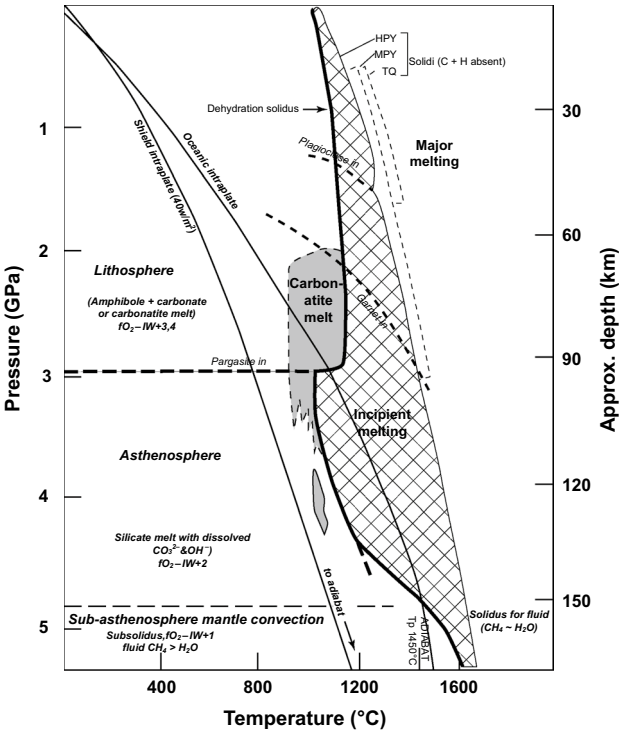

Fig. 12 A model for the Earth's uppermost mantle in *intraplate* locations and emphasising young continent or oceanic crust and lithosphere. The model is based on experimental determination of phase assemblages, solidus and melt compositions of lherzolite and assumes minor carbon and hydrogen (water) in the upper mantle and decreasing oxygen fugacity with increasing depth. A field for carbonatite melt is shown, but it is suggested that this melt is very mobile, even at very small melt fraction and migrates along the geotherm to the decarbonation boundary. Conditions are subsolidus (hydrous silicate melt) to ~90 km defining the *lithosphere* but at this depth the geotherm enters a *P*, *T* field for incipient melting (the *asthenosphere*) the melt being a carbonate-bearing olivine + melilite nephelinite. The depth of the lithosphere/asthenosphere boundary (LAB) is stable against *T* variation of ~100 °C due to the steep negative d*T*/d*P* of the pargasite breakdown (dehydration solidus). The lower boundary of the asthenosphere is assumed to be the second intersection of the geotherm and lherzolite solidus which will depend on the CH_4/H_2O of the C, H, O fluid. Slow upward migration of the near-solidus melt within the asthenosphere produces a depth interval of enrichment (*upper*) and depletion (*lower*) in incompatible elements, particularly H, C, P, K. Consequently, there is a decoupling of major elements and incompatible trace elements. The figure illustrates the argument that the phase relationships and melting behaviour of fertile or enriched lherzolite are a necessary and sufficient condition for the LAB and enable the plate tectonics behaviour of the Earth (Green and Falloon 2005)

A model for the intraplate upper mantle

The complexity of lherzolite melting in the upper mantle which is illustrated in Fig. 10 suggests a need to choose a model of oxygen fugacity variation with depth (Fig. 12), thus predicting where melting will occur and the nature of the melt and residue fractions. In addition, different tectonic

settings may be characterised by different oxygen fugacity, e.g. island arcs vs mid-ocean ridges. The appropriateness of such models with respect to the real Earth can be assessed by their consistency with petrological, geochemical and geophysical observations. In Fig. 12 (Green and Falloon 1998, 2005), depicting an intraplate setting, oxygen activity decreases with depth in the upper mantle in intraplate settings with the lithosphere having fO_2 ~ FMQ (IW + 3–4 log units). This is supported by studies of spinel in lherzolite xenolith suites and in high-temperature lherzolite intrusions showing decompression histories. The evidence for invasive sodic dolomitic carbonatite melts at ~1.5–2 GPa, crossing the decarbonation reaction to react with enstatite yielding high Ca/Al lherzolite and wehrlite, and releasing CO_2 fluid, has been demonstrated by studies of xenolith suites from several localities including SE Australia and New Zealand (Yaxley and Green 1996; Yaxley et al. 1998; Scott et al. 2014). Similarly, the presence of pargasite (or glass-rich pools from high-temperature decompression melting of pargasite during magmatic transport) and CO_2-rich fluid inclusions in spinel lherzolite xenolith suites is consistent with Fig. 12.

In the model of Fig. 12, the oceanic intraplate geotherm is subsolidus (i.e. pargasite ± dolomite lherzolite) to ~70 km and then enters the field of pargasite-bearing garnet lherzolite with sodic dolomitic carbonatite melt from ~70 to 95 km. In SE Australia and in other intraplate areas of young volcanism (Scott et al. 2014), examples of lherzolite xenoliths provide evidence of sodic, dolomitic carbonatite melt metasomatism. Mineral compositions indicate conditions near 60 km, 1,000–1,100 °C, cooling to ~800 °C, i.e. cooling from a perturbed geotherm in the spinel lherzolite rather than garnet lherzolite stability fields (O'Reilly and Griffin 1985). In this example, perturbation of the geotherm is attributed to the mantle upwelling and intermittent volcanism associated with lithospheric thinning and separation of the Australian and Antarctic plates. An unresolved issue in the model of Fig. 12 is whether carbonatite melt at 70–95 km depth has similar or much faster porous flow rate (i.e. melt permeability) in comparison with hydrous silicate melt at similar porosity.

In oceanic intraplate settings and the depth range from 60 to 150 km, fO_2 is assumed to decrease from fO_2 ~ (IW + 3–4 log units) to fO_2 ~ (IW + 1 log units) with the consequence that carbonate is no longer stable and is replaced at subsolidus temperatures with graphite + water-rich vapour. Pargasite also breaks down at ~95 km so that if >200 ppm H_2O is present, the lherzolite solidus for hydrous, carbonate-bearing silicate melt drops sharply to ~1,000 °C. The model oceanic geotherm enters a region of incipient melting in which the melt fraction present is primarily determined by the H_2O content. The character of the melt is very silica-undersaturated olivine melilitite to olivine nephelinite. Porosity and permeability are important in determining whether a small melt fraction is rapidly extracted or is effectively trapped over geologically significant time scales. The experimental studies by Faul (2001) show a sharp increase (1–2 orders of magnitude) in permeability for silicate melt as the melt fraction exceeds ~2 wt%. It is hypothesised that at melt fractions less than ~2 wt%, carbonate-bearing, hydrous silicate melt is effectively 'trapped' or moves slowly in comparison with rates of mantle upwelling. In intraplate settings, it is assumed that this incipient melt can migrate upward for 100–200 km by porous flow on time scales of 10–100 M yrs (0.1–2 cm/yr). If this occurs, melt migrates along the geotherm to the pargasite stability boundary, i.e. the migrating melt is either ponded (enhanced melt layer) at ~95 km depth or reacts and freezes at <95 km as pargasite-enriched lherzolite. If the migrating melt contains dissolved carbonate, then the pargasite-forming reaction at ~95 km is accompanied by the release of a carbonatite melt fraction or by the precipitation of graphite, depending on ambient fO_2.

The understanding of melting in lherzolite + (C, H, O) at depths greater than ~95 km involves knowledge of the solubility of water in nominally anhydrous olivine, pyroxenes and garnet (NAMs), the maximum solubility of water in silicate melts as pressure increases and the liquidus depression of appropriate silicate melts as a function of water content. In experimental studies of the model mantle composition HZ sandwiched between monomineralic layers of olivine and/or pyroxene, the water contents of olivine and pyroxenes at the vapour-saturated lherzolite (HZ) solidus were determined (Green et al. 2010, 2011, 2014; Kovacs et al. 2012). The maximum water content in lherzolite NAMs at the vapour-saturated solidus at 2.5 GPa and 4 GPa is ~200 ppm at ~1,010 and 1,210 °C, respectively. The near-solidus melt compositions are olivine-rich and strongly nepheline-normative, and although the water content of the melt cannot be determined directly, it can be inferred to be 25–30 wt%. This inference derives from studies of solubility of water and consequent liquidus depression by different water contents in a variety of olivine-rich mantle-derived magmas (peridotitic komatiite, olivine-rich basanite, olivine leucitite, olivine melilitite) (Fig. 13).

Experimental studies of HPY, MPY and Tinaquillo lherzolite derived melt composition and melt fraction as a function of temperature for anhydrous melting (Jaques and Green 1980; Falloon and Green 1987, 1988) at pressures to 3.5 GPa. The melt fraction vs temperature relationship at 1.5 to 3 GPa (Fig. 14a, b) is approximately linear with low-degree melt fractions being mildly nepheline-normative and in equilibrium with lherzolite to harzburgite residue, clinopyroxene being eliminated from the residue at 10–15 % melting. Melt compositions increase in normative olivine with increasing pressure. Melting in the presence of water

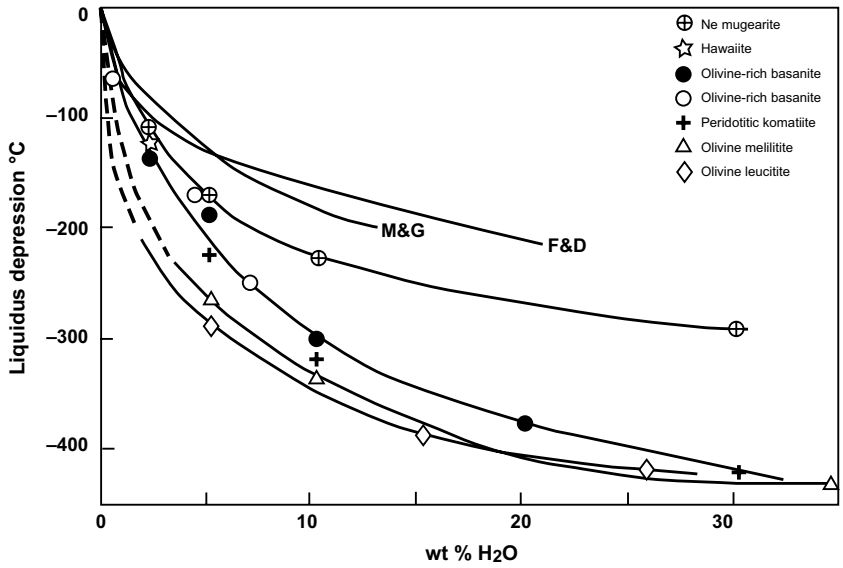

Fig. 13 Experimental determination of the liquidus depression in olivine-rich magmas as a function of dissolved water at high pressure. Data from experimental studies in which the anhydrous and water-saturated liquidi have been determined at several pressures (Green et al. 2014)

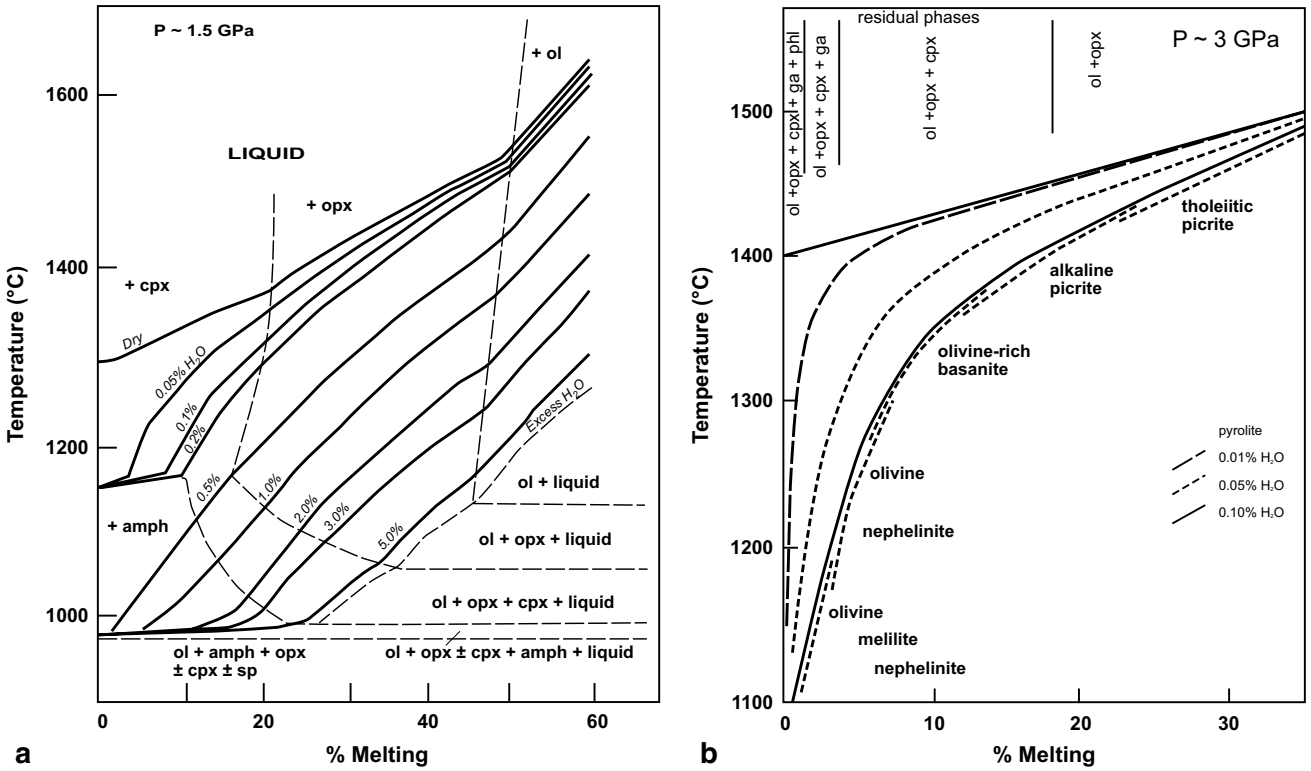

Fig. 14 Melting in a hydrous mantle—an early parameterization of the relationship between melt fraction, temperature and water content of the source lherzolite. **a** At about 1.5 GPa where pargasite is stable at the solidus, and for low water contents (<3,000 ppm approximately), the solidus is ~1,150 °C. Note the formation of ~10 % melt over a very small temperature interval if the mantle contains 2–3,000 ppm H_2O, i.e. 15–20 % pargasite below the solidus (Green 1972). **b** At about 3 GPa where pargasite is not stable at the solidus (Green 1971)

begins at 250–300 °C lower temperature, and melt fraction vs temperature relationships are strongly dependent on water content (Fig. 14a, b). The partitioning of water between residual lherzolite (~200 ppm) and hydrous silicate melt (~25–30 wt%) is estimated as D_{H2O} ~ 0.0006, i.e. water is extremely incompatible in mantle melting, similar to K_2O, P_2O_5, LREE, etc. For a given melt fraction, water partitioning (D_{H2O}) and bulk water content, the water content

in the melt can be estimated. Although the compositions of melts will differ between dry and 'wet' melting, all melts will be olivine-rich at >1 GPa and the liquidus depression for a given water content is similar whether for a low-degree alkali-rich melt or a high degree komatiitic melt (Fig. 13). Thus, an empirical relation between melt fraction, temperature and mantle water content can be derived for hydrous melting. Figure 14a, b presents early models of hydrous melting at 1.5 and 2.5 GPa based on the experimentally determined solidus for lherzolite and experimental studies of water solubility and liquidus depression on a variety of basaltic compositions. More recent numerical models produce similar figures (e.g. Katz et al. 2003, Figs. 9, 10) but do not include the important role of pargasite in controlling the solidus to 3 GPa for small water contents.

In parallel with experimental studies of the melting behaviour of lherzolite (+C, H, O), the 'inverse' approach to understanding mantle petrogenesis explored the liquidus phases of mantle-derived ('primary') magmas as functions of P, T and C, H and O contents. The goal of such experimental studies is to find P, T, fO_2 and dissolved C–H–O species, for which the proposed 'primary' magma is in equilibrium with residual phases of peridotite, i.e. olivine + orthopyroxene ± clinopyroxene ± (Al-rich phase plagioclase, spinel or garnet). Noting the large chemical variation of volcanic rocks, including glasses, the selection of 'primary' magma compositions for experimental testing is based on magmas which contain xenoliths of mantle origin (density >3.3 gm/cc) and which also have $Mg^{\#} = 70–75$, i.e. having liquidus olivine with $Mg^{\#} = 89–93$. These two constraints avoid magmas which have partially crystallized and fractionated (including high-pressure fractionation within the mantle) before xenolith capture and eruption. This approach is appropriate for intraplate magmas from alkali olivine basalts to olivine melilitites, olivine leucitites and kimberlites, i.e. nepheline-normative primary magmas (Green 1973a; Brey and Green 1977; Adam 1990). However, the tholeiitic (hypersthene-normative) basalts of mid-ocean ridges, intraplate or arc settings do not contain mantle xenoliths and require a different approach to identifying 'primary' magmas. For these magmas, we seek the most Mg-rich glass compositions and the most magnesian olivine phenocrysts or microphenocrysts within the glass. Using the known distribution of Mg/Fe between olivine and melt, the liquidus olivine composition is iteratively added to the glass composition to calculate a parental or 'primary' composition in equilibrium with the observed most Mg-rich microphenocryst. In this way, 'primary' tholeiitic picrite magmas for mid-ocean ridges and 'hot-spots'(OIB) have been inferred and conditions of equilibration with residual harzburgite (with very minor subcalcic clinopyroxene and Al–Cr spinel) determined (Figs. 1, 15a, b).

The integration of both forward and inverse experimental approaches to the understanding of melting in the upper mantle (i.e. studying both a model lherzolitic upper mantle composition and mantle-derived magmas) and emphasising the roles of water and carbon is summarised in Fig. 15a, b. In Fig. 15, the field for carbonatite melt (Fig. 12), discussed previously, is not shown and attention is focussed on the role of water, pargasite and hydrous silicate melt (with dissolved $CO_3^{=}$). The two mantle compositions which are compared are suggested as MORB source (Fig. 15a) and intraplate rift or OIB source (Fig. 15b), i.e. MORB Pyrolite/HZ1 lherzolite, and Hawaiian Pyrolite of Table 1. They have similar major element compositions but differ in water content and minor and trace elements. Differences in subsolidus mineralogy are principally in pargasite contents. Based on the experimental studies described earlier, it is assumed that ~200 ppm water remains in residual NAMs at the solidus at >3 GPa and that this residual water decreases with increasing temperature and melt fraction at any pressure. The water contents in both examples are such that all water is stored in pargasite + NAMs at <3 GPa, but the sharp inflexion of the pargasite solidus (dehydration solidus) means that the intraplate geotherm crosses the solidus at ~90 km depth. The intraplate geotherm traverses the field of incipient melting with melt fraction strongly dependent on water content.

The mobility of the incipient melt fraction (i.e. <1–2 %) determines the fractionation and abundance of incompatible elements, particularly for elements with $D_{\text{residue/melt}} < 0.01$, for mantle regions where there is partial melting controlled by volatile elements, particularly C, H, O. The permeability of lherzolite with a very small melt fraction is complex in theory and poorly constrained by experiment. Theoretical controls include melt viscosity, melt density, surface interaction between melt and crystalline phases, and melt distribution (i.e. edge location as tubules, surface layers and interserts). Experimental studies of silicate melt in dunite (Cmiral et al. 1998; Faul and Jackson 2007; Faul. 2001; Garapic et al. 2013) reveal melt distribution in surface films, tubules (grain edges) and interserts bounded by multiple crystal faces, even at very small melt fraction. Faul (2001) found a large increase in permeability at 1–4 % melt and argued that silicate melts at lower melt fraction were not readily mobile under conditions of incipient melting. A small (~1 %) melt fraction could also be retained in residual harzburgite or lherzolite after major melting such as a mid-ocean ridges. Faul and Jackson (2007) found increased strain rates by ~2 orders of magnitude due to melt fraction of 1–2 % melt, relative to dry, melt-free dunite. Taken together, these observations imply that there is a sharp decrease in melt mobility at <1–2 % melt fraction melt and, furthermore, that regions with incipient 'trapped' melt are rheologically 'weak' and of much lower viscosity

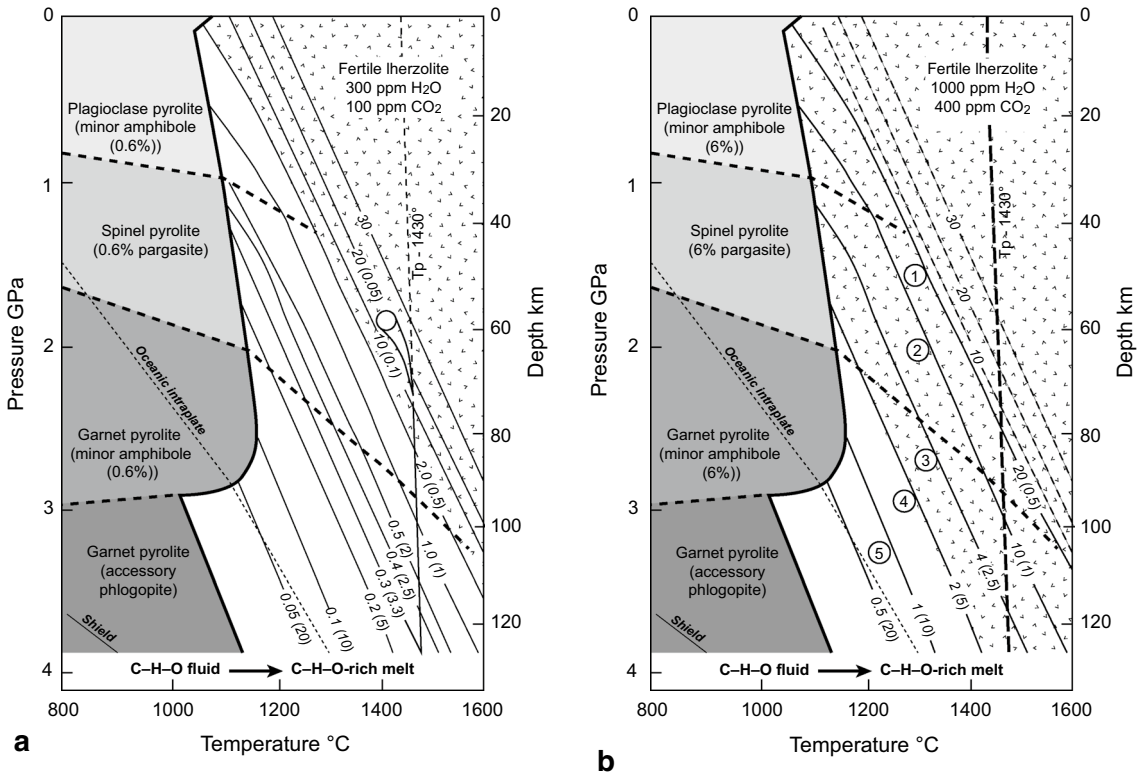

Fig. 15 Major melting and incipient melting regimes for fertile (MPY) and enriched (HPY) lherzolites with assumed water and CO_2 contents (Green and Falloon 2005). **a** Solidus and melting parameterization for model MORB-source mantle with 300 ppm H_2O and 100 ppm CO_2, mantle potential temperature (T_p) of ~1,430 °C. *Contours* show % melt and approximate dissolved water content of melt (in *brackets*). A permeability threshold (sharp increase) at ~2 % melting contour is marked by shading. Parental MOR picrite from ~15 % melt at ~2 GPa, 1,420 °C. **b** Solidus and melting parameterization for model intraplate (enriched–HPY) mantle with 1,000 ppm H_2O and 400 ppm CO_2, mantle potential temperature (T_p) of ~1,430 °C. Solid line contours show % melt from 0.5 to 20 % and approximate dissolved water content of melt (in *brackets*). Shaded area denotes >2 % melt. *Dashed line* contours refer to MORB-source mantle. Primitive and mantle xenolith-bearing basalts from SE Australia at inferred depths of melt segregation: *1* olivine tholeiite, *2* alkali Ol. basalt, *3* Ol-rich basanite (Green 1973a), *4* Ol-Nephelinite, *5* Ol-melilite-nephelinite (Frey et al. 1978)

than subsolidus lherzolite (including water in NAMs and hydrous phases such as pargasite or phlogopite). These conclusions are used in Figs. 7, 12, 15, 16 and 17 to derive models for the asthenosphere, MOR, intraplate, 'hot-spot' and convergent margin magmatism.

Origin of MORB

For MORB-source mantle (Fig. 15a) assumed to contain ~300 ppm water and ~100 ppm CO_2, the melt fraction along the geotherm is extremely small (0.05–0.1 % melt), and as previously discussed, this melt is relatively immobile. In Fig. 15a with bulk water content of 300 ppm, we assume ~100 ppm water enters the melt phase near the solidus. Contours of melt fraction and water content in melts are approximate and based on D_{H2O} ~ 0.0006 (residue/melt), and liquidus depression by dissolved water from Fig. 13. Due to the positive dT/dP of the water-saturated solidus (possibly enhanced by decreasing fO_2 with increasing depth), the intraplate geotherm re-crosses the vapour-saturated solidus at 150–250 km (Figs. 7, 12). In Fig. 15a, adiabatic upwelling from the *lower part of the incipient melting interval* is illustrated along a mantle adiabat for potential temperature (T_p) ~ 1,430 °C. The selection of T_p ~ 1,430 °C is based on the evidence for picritic parental magmas for the most primitive MORB. During upwelling, water content of residual minerals decreases as water partitioning between NAMs and melt changes as functions of both temperature and melt composition. The 2 % melt contour in Fig. 15a lies close to the anhydrous solidus and with further upwelling melt fraction increases rapidly. Adiabatic upwelling is depicted as producing parental MOR picrites segregating from residual lherzolite to harzburgite (olivine + orthopyroxene ± clinopyroxene + Al–Cr spinel) at ~20 % melting. It is important that if the upwelling mantle from the lower part of the asthenosphere remains a closed system (a diapiric rather than continuous flow model), then the incompatible element contents (including water and

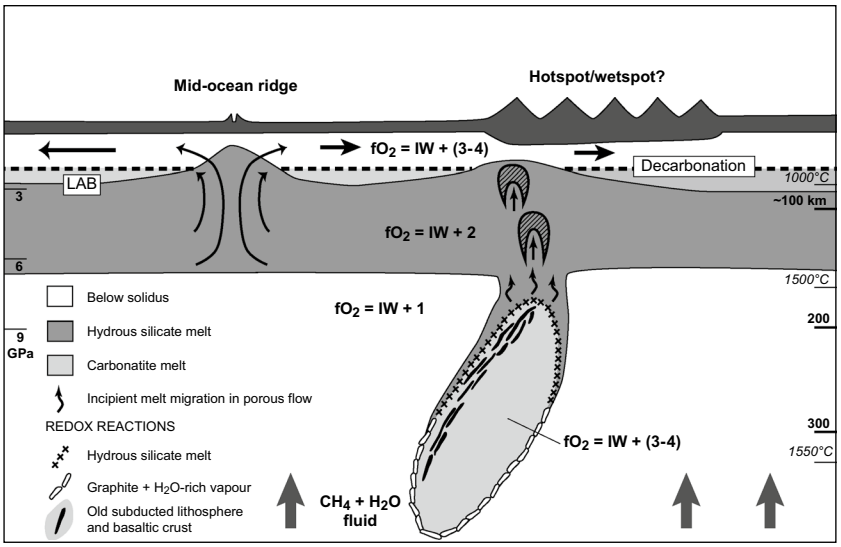

Fig. 16 Diagram suggesting a model for intraplate 'hot-spot' or island chain volcanism, in which the cause of the volcanism is 'fixed' relative to lithospheric plate movement. The model attributes the cause of the long-lived melting anomaly to compositional heterogeneity within the mantle beneath or within the lowermost part of the asthenosphere. Specifically, the compositional heterogeneity is suggested to be old subducted slab(s) and the interface between such slabs and ambient mantle is a redox contrast at which f_{H2O} is a maximum, triggering melting at the vapour-saturated solidus for lherzolite with graphite/diamond and water-rich fluid. The near-solidus melts are depicted as lowering viscosity to permit diapirism in which mixing and reaction occurs between asthenospheric mantle and old subducted crust + lithosphere. Melt segregation within upwelling mantle occurs at shallower depths and higher melt fraction. Although the model suggests a temperature anomaly ('plume') at shallow depths in the lithosphere and asthenosphere, there is no deep-seated thermal plume and the melting anomaly is effectively due to higher (C, H, O) contents and chemical heterogeneity of the old subducted slab/ambient mantle interface (modified from Fig. 7.12 in Green and Falloon 1998)

carbon) of the MOR picrite are determined by high degrees of melting of residual, depleted lherzolite, i.e. with little fractionation of incompatible elements by the melt segregation process. The moderately depleted to highly depleted incompatible element contents of N-MORB to D-MORB are interpreted as characteristic of the lower asthenosphere. This has experienced one or more episodes or 'continuous' loss of incipient melt fraction at the vapour-saturated solidus (water-rich vapour) at 4–7 GPa. Correlations between water and incompatible elements and correlations among trace elements reflect source compositions which are residues from earlier, pre-upwelling, loss of hydrous and carbonate-bearing silica-undersaturated melts from garnet lherzolite near the vapour-saturated solidus at >4 GPa.

Origin of intraplate basalts

For intraplate basalts (Fig. 15b), higher water (1,000 ppm) and CO_2 (400 ppm) contents of the source are assumed so that contours of degree of melting illustrate a higher melt fraction along an intraplate geotherm. Figure 15b presents a scenario for intraplate rifting in which upwelling from the middle and upper levels of the asthenosphere produces magmas matching the primary xenolith-bearing magmas from olivine melilitite to alkali olivine basalts. The degree of silica-undersaturation increases with higher volatile contents ($H_2O + CO_2$), decreasing temperature and melt fraction and increasing pressure of melt segregation (see Fig. 15b). Larger melt fractions yield intraplate olivine tholeiites by upwelling from deeper levels and higher temperatures on the geotherm. This may also imply greater lithospheric thinning. The assignment of magma types to particular pressures, temperatures and volatile contents [i.e. melt fraction for source with a given ($H_2O + CO_2$) content] is based on the experimental studies of intraplate magmas at various *P*, *T* and volatile contents. The petrogenetic model of Fig. 15b is suggested for *limited* intraplate rifting of continental crust and lithosphere, which does not continue to the formation of new oceanic crust. The major element and incompatible element contents of mantle-derived, xenolith-bearing basalts of Tertiary to Recent age in Victoria/Tasmania require source compositions which are enriched relative to chondritic or N-MORB abundances (Frey et al. 1978). This is a region of subcontinental lithospheric thinning as the Australian plate diverged from the Antarctic plate. Enrichment in the base of the lithosphere or in the upper asthenosphere is also suggested for oceanic sea mounts in locations where lithospheric stress due to adjacent subduction leads to small-scale young volcanism on old oceanic lithosphere ['petit-spot' volcanism of Hirano et al.(2006)]. Magmas of this setting have very high volatile ($H_2O + CO_2$), and alkali contents and some contain mantle xenoliths.

'Hot-spot' basalts

In the plate tectonics paradigm, a distinctive type of volcanism is designated 'Hot-spot volcanism', readily seen in oceanic intraplate settings but also occurring on continents and crossing continent/ocean boundaries. 'Hot-spot' volcanism produces linear volcanic chains with, ideally, monotonic age progression, and chain orientation reflecting plate movement over a stationary magma source. Initial interpretations of 'hot-spot' traces on different plates suggested a fixed reference frame for major 'hot-spots' and the high rate of magma eruption at Pacific plate 'hot-spots' suggested high melt fractions, equated with high temperatures and a continuously supplied magma source. 'Hot-spot' volcanism is commonly attributed to narrow, thermally buoyant plumes sourced below the lithosphere and asthenosphere, possibly from a core/mantle boundary layer (Morgan 1971; Davies 1998). The 'deep mantle plume' hypothesis is widely applied in geodynamic and geochemical literature and has developed to include recognition of geochemical signatures of old subducted basaltic and continental crust in the upwelling plume. A central tenet in the hypothesis is the requirement for thermally induced buoyancy for the mantle plume with a temperature excess of >200 °C for the upwelling plume relative to ambient mantle. 'Hot-spot' magmas are interpreted as melt products of mantle plumes, the high magma flux and diverse geochemical fingerprints reflecting the excess temperature and plume source imparted from a core/mantle boundary layer built up from old subducted slabs. The hypothesis has become more complex with further studies and come under critical assessment (Foulger 2007, 2010). A testable prediction from the 'deep mantle plume' hypothesis is that primary 'hot-spot' magmas are a product of higher-temperature upwelling than primary MORB, i.e. they are from greater depths and melt fraction, reflecting the lherzolite solidus intersection with the respective adiabats for plume source and normal mantle. The examination of MORB glasses and olivine microphenocrysts previously summarised led to identification of primary picrite magmas and to the inference that upwelling and magma segregation at mid-ocean ridges requires an adiabat of ~1,430 °C. A similar examination of Hawaiian glasses and phenocrysts as representative of a well-studied 'hot-spot' shows that primary magmas are also picrites and that liquidus temperatures are significantly lowered by greater dissolved ($H_2O + CO_2$) contents relative to MOR picrites. Using the magmas as probes to mantle temperature and source composition, there is no evidence for excess temperatures of ~200 °C at 'hot-spot' sources. The 'plume' adiabat is similar or lower temperature than ambient mantle as sampled in the mid-ocean ridge settings. The compositions of 'hot-spot' primary magmas indicate similar to higher melt fractions (or more harzburgitic source) and harzburgite (Ol + Opx + Cr-spinel) rather than lherzolitic (Ol + Opx + Cpx + Al–Cr spinel) residues. In detail, the individual Hawaiian shield volcanoes show distinctive Opx-controlled trends in normative projections of magnesian glasses, indicative of variability in the source composition. Some of this variability (lower Ca/Al and higher Na and Si contents) is interpretable as mantle re-fertilisation by partial melts from subducted oceanic crust, i.e. an 'arc' signature from refertilisation by adakitic melt from eclogite.

Using the major element compositions of the most magnesian glasses and phenocrysts of both MORB and 'hot-spot' tholeiitic magmas and their phase relations at high pressure, it is argued that there is no evidence for a deep thermal anomaly as the cause of 'hot-spot' volcanism. However, there is evidence for compositional 'anomaly' in major and minor elements, re-enforced by trace element and isotopic heterogeneity. The chemical heterogeneity includes evidence for old subducted crustal components in the source. The 'deep mantle plume' hypothesis postulates that cool subducted slabs accumulate at the core/mantle boundary, are heated there and convectively rise as thermally buoyant plumes. An alternative model that is consistent with the evidence for similar temperatures and depths of magma segregation for both MOR and 'hot-spot' primary magmas is illustrated in Fig. 16. The mantle (peridotite) component of subducted slabs is initially cool and negatively buoyant. However, if it is depleted to refractory (Table 2) in composition, then it will become neutral to positively buoyant as the temperature of the subducted slab approaches ambient mantle. Figure 16 depicts old subducted slabs suspended below or within the asthenosphere and providing a locus for melting, particularly at interfaces where there is a redox contrast between ambient mantle (at fO_2 ~ IW + 1 log unit) and oxidised and carbonate-bearing old subducted slab. At such interfaces in (C, H, O)-bearing lherzolite, carbon is precipitated, water activity is at a maximum, and melting produces carbonate-bearing hydrous silicate melts (provided temperatures at the interface are above the vapour-saturated solidus for water-rich vapour at graphite/diamond saturation) (Fig. 16). Movement of such melts into overlying asthenosphere, or upwelling from the interface region itself, leads to diapirism and segregation of large melt fraction at 1.5–2.5 GPa, i.e. 'hot-spot' magmatism.

In the model presented here, the major and minor compatible elements of magmas are determined by the phase relations at the P, T of magma segregation. For olivine tholeiite or picrite magmas, the major element compositions and liquidus phases require a high degree of melting of fertile lherzolite. Residual olivine, enstatite, spinel and possibly minor clinopyroxene do not cause fractionation among the incompatible elements. Thus, the large

fractionations among incompatible elements observed, for example, between D-MORB, N-MORB, E-MORB and OIB are attributed to differences in 'source composition'. An example of the disconnect between petrogenetic inferences from major element and incompatible element data is the Kilauea-Iki (1959–1960) eruption of olivine tholeiite. Glass, olivine and bulk compositions argue for a picritic parental composition, and experimental studies show that this has olivine and orthopyroxene as liquidus phases at ~2 GPa implying harzburgite residue and magma segregation at ~60–70 km depth. This is consistent with observation of pre-eruption seismic tremor migrating from this depth to surface eruption. However, incompatible elements (particularly LREE) are enriched relative to N-MORB or chondritic abundances and imply residual garnet and low percentage melt. Reconciling both major element and incompatible element constraints requires prior source enrichment at high pressure by a highly incompatible-enriched small melt fraction. The incompatible and isotopic compositions are controlled by addition or depletion of incipient melt components, i.e. of hydrous, carbonated silica-undersaturated melts from near-solidus garnet lherzolite + (C, H, O). If this model is correct, then we cannot use incompatible trace element abundances to infer melt fraction and residual mineralogy, particularly assuming a bulk composition with N-MORB or chondritic relative abundances (see also Niu et al. 1996). Rather, the petrogenesis of 'hot-spot', intraplate and MOR primary magmas includes major element and compatible element compositions determined by *P*, *T* and melt fraction and incompatible element and related isotopic compositions determined by the addition or depletion of incipient melt fractions (including wall rock reaction and melt migration in the asthenosphere). In Fig. 16, redox reaction at interfaces between old subducted slab (including eclogite, carbonate and refractory harzburgite) and ambient mantle precipitates carbon and increases H_2O activity. Locally derived small melt fractions with garnet lherzolite residue will form at such interfaces if temperatures (at ~200 km for example) are higher than 1,375 °C (Fig. 7). The 'hot-spot' source compositions are envisaged as mantle enriched by addition(s) of these melts carrying distinctive and complex incompatible element and isotopic ratios. Rather than 'hot-spot', the island chain volcanism might preferably be called 'wet-spot', reflecting the presence of higher water and carbonate contents, attributed to the influence of old subducted slabs within or beneath the base of the asthenosphere.

Magma segregation and wall-rock reaction

The parallel studies of melting of model mantle lherzolite + (C, H, O) and basaltic (tholeiitic to melilititic) magmas provided the phase equilibria basis for the petrogenetic models of Figs. 13, 14, 15 and 16. Intrinsic to these models is the concept of a 'depth of magma segregation' at which a particular primary magma separates from residual peridotite. Following segregation of a primary magma, olivine (±Cr-spinel) is its liquidus phase at lower pressure, and if it flows through a dunite channel at deep levels or chilled margin dyke at shallow depths, then the magma remains a closed system to further change in major or minor compatible element composition. In this case, the magma composition retains the signature of its depth of segregation. This model of mantle upwelling, decompression melting and magma segregation is appropriate for dynamic upwelling or diapirism in which the instability of a geothermal gradient which is steeper than the adiabatic gradient, coupled with the lower viscosity and density of the asthenosphere, leads to episodic buoyant diapirs. If such diapirs ascend at near-adiabatic conditions, then the temperature contrast between diapir and ambient mantle increases and the increasing melt fraction is 'sealed' within the diapir until a breaching of pargasite lherzolite carapace and draining of the melt occurs through dunite channel/dyke system. These concepts are illustrated in Fig. 17b–d. Also, noting the sensitivity of incompatible element abundances and related isotopic ratios to addition or loss of a very small hydrous and carbonatitic melt fraction, Fig. 17b illustrates a cooling and shrinking diapir in which melt fraction increases without wall-rock reaction. Figure 17c, d illustrates a diapir heating and extracting a small melt fraction from the lithospheric wall rock with addition also of incipient melt from the uppermost asthenosphere in Fig. 17d. The nature of melting in Fig. 17b–d approaches 'batch melting' with possible addition of incompatible element-enriched melt from wall-rock reaction.

In contrast to the dynamic upwelling models, Fig. 17a illustrates 'passive upwelling' as suggested for MOR settings, particularly fast-spreading ridges. In this model, whole lithosphere is newly formed by asthenospheric

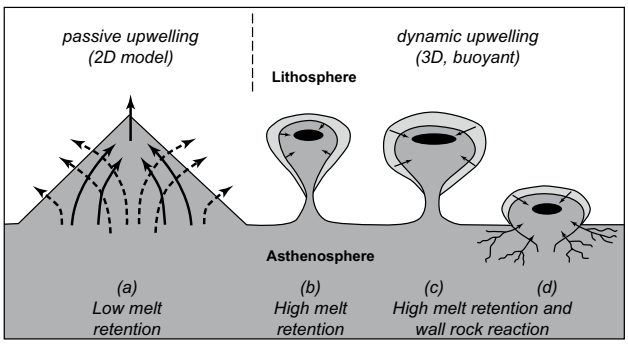

Fig. 17 Diagram illustrating several aspects to the understanding of mantle upwelling, decompression melting and magma segregation in MOR and intraplate settings (From Fig. 7.9 in Green and Falloon 1998)

upwelling with melt aggregating by porous flow and melt focussing as diagrammatically illustrated. The melt is considered to be mobile even at very small melt fraction, and final melt compositions erupted represent aggregations of melt increments from the whole melting volume. The model does not appear to address the issues of continuous 'back reaction' of melt experiencing porous flow, or the evidence for threshold permeability at 1–2 % melt.

Models of convergent margin volcanism

Plate tectonics includes the subduction and return to the mantle of oceanic crust and lithosphere, creating greater complexity in *P*, *T* conditions and compositions than in either intraplate or mid-ocean ridge settings. Seismological evidence argues for the persistence of the cool subducted slab to the transition zone, and arguably into the lower mantle. There are many models of temperature distribution in the slab and overlying mantle wedge, influenced by subduction rate, trajectory and age of subducted slab. Insight into possible melting processes and products can be gained by overlaying model temperature profiles with the relevant phase assemblages and solidi for the mix of lithologies present in slab and mantle wedge. Oceanic crust and lithosphere is inferred to be variably hydrated, oxidised and carbonated, and subduction leads to progressive metamorphism and dehydration, particularly of high pressure, low-temperature character. Temperature distributions in slab and overlying mantle wedge argue that melting of peridotite is most likely in the mantle wedge, with solidi lowered by access of slab-derived fluids or melts. Melting is also likely in subducted crust juxtaposed against overriding, high-temperature lithosphere along the Benioff Zone because the solidi of basaltic or sediment compositions, including both water-saturated solidi and dehydration solidi, are at lower temperature than peridotite solidi. A similar juxtaposition of contrasted lithologies against high-temperature mantle may occur at subduction zone/transform fault intersections. Figure 18a, b illustrates some of the processes acting in the convergent margin environment as inferred from phase equilibrium experimental studies. At low temperatures, reactions in oceanic crust lead to fluid ($H_2O + CO_2$) migration into overlying mantle wedge (fore-arc) and some of this material may be entrained with the subducted slab. Average basaltic crust composition reacts to quartz (coesite) eclogite with amphibole, phengite or paragonite, and dehydration melting at 700–850 °C at 1.5 to 2.5 GPa yields water-rich $(CO_3)^{=}$-poor melts of dacitic to rhyodacitic composition. If minor carbonate is present, then it may remain as a residual phase carried to greater depths within the slab, whereas the hydrous dacitic melt (adakite) may migrate into the overlying mantle wedge (Fig. 18b). Particular attention is drawn to the prediction of carbonatite melts in peridotite within the mantle wedge (Green et al. 2004; Tumiati et al. 2013). Because of the temperature inversion within the mantle wedge and the oxidised and carbonate-bearing character of oceanic crust and entrained sub-fore-arc mantle, the solidus for carbonatite melt in peridotite + H_2O + CO_2 at ~930 °C, 3 GPa is exceeded before the appearance of carbonated, hydrous silicate melt at ~1,025 °C, 3 GPa (Fig. 18b). A region of carbonatite melt in lherzolite/harzburgite lies beneath the region of water-saturated melting in the mantle wedge. The scenarios outlined in Fig. 18a, b and Tumiati et al. (2013) emphasise the importance of the inverted temperature profile in the mantle wedge overlying the subducted slab. This has the consequence that a carbonatite melt (with or without coexisting water-rich fluid) may migrate up-temperature, crossing the solidus for hydrous, carbonated silicate melt in harzburgite/lherzolite of the mantle wedge. Melt fraction will increase and dissolved volatiles will decrease as melt percolates to higher temperature in the core of the wedge. Upwelling or diapirism from within the mantle wedge will increase the melt fraction, and residues become harzburgitic with high $Mg^{\#}$ and $Cr^{\#}$ in olivine and spinel, respectively. Upwelling to shallow depths or magma segregation and ascent will lead to vapour saturation and loss of (C, H, O) fluid due to decreasing solubility of CO_2 particularly at pressures below 1.5 to 1 GPa. As a consequence of degassing during ascent, primary magmas must begin crystallisation at depth and will commonly fractionate prior to eruption. Nevertheless, primitive magmas contain highly magnesian olivine phenocrysts (to Fo_{92}–Fo_{94}) and some provide evidence for distinctive conditions of genesis. Examples include low-calcium quartz-normative boninites with magnesian olivine, protoenstatite ($Mg^{\#} = 92$–93) and chromite ($Cr^{\#} > 85$) which have major and minor element compositions indicating fluxed melting at T ~ 1,300 °C of mantle-wedge harzburgite. The access of hydrous dacitic melt (adakite) with high Na/Ca, Al/Ca into a refractory and high temperature mantle wedge is suggested. Low-Ca boninites, in particular, seem to require the introduction of both Na_2O and H_2O in a slab-derived melt (rather than aqueous fluid) and particularly refractory harzburgite in the mantle wedge. In contrast, distinctive island arc ankaramites or ankaramitic picrites contain clinopyroxene phenocrysts to $Mg^{\#} = 93$–94, coexisting with olivine ($Mg^{\#} = 92$). Magma compositions have Na and Ca enrichment relative to Al. Experimental studies demonstrated that such magmas could be partial melts from lherzolite to harzburgite sources by melting with ($H_2O + CO_2$), i.e. by melting in the mantle wedge fluxed by carbonatite melt and aqueous fluid as illustrated in Fig. 18b (Green et al. 2004). The brief discussion of melting in convergent margin environments illustrates the complexity generated by overlaying

phase equilibria, including melting with CO_2 and H_2O, on the model temperature profile of subducted slab and mantle wedge. The following processes are important.

1. Volatiles, particularly water, transfer from subducted slab to overlying, higher-temperature mantle wedge.
2. Melting occurs under oxidising conditions (fO_2 >/= IW + 3, 4 log units).
3. Melting may occur in subducted crustal lithologies (eclogite) at temperatures below the peridotite solidi leading to slab to wedge 're-fertilisation' by adakitic melts.
4. Melting of carbonated peridotite may occur within the mantle wedge at temperatures below the water-saturated solidus. Carbonatite melts may cause distinctive 're-fertilisation' signatures and also lead to island arc ankaramitic magmas.
5. The peridotite compositions available for fluxed melting in the mantle wedge environment (as in 1–4 above) include much more refractory compositions than are available in MORB or intraplate settings. As a consequence liquidus phases of primary melts and residues from melt extraction may be more refractory i.e. higher $Mg^{\#}$ in olivine, orthopyroxene and clinopyroxene, higher $Cr^{\#}$ in spinel, higher An content in plagioclase. Orthopyroxene-rich magmas with very Cr-rich spinels and with distinctive high MgO, SiO_2 and low CaO contents imply fluxed remelting of harzburgitic rather than lherzolitic mantle (Fig 7.14, Green and Falloon 1998).
6. Highly incompatible element and related isotopic ratios in primitive magmas reflect multiple processes in precursor histories of slab or wedge.
7. Primary magmas may initially be vapour-undersaturated but with decreasing pressure, vapour saturation, vesiculation and crystallisation of liquidus phases are unavoidable, particularly for magmas with dissolved carbonate (island arc ankaramites). The presence of a methane component in the escaping fluid leads to oxidation in the melt.

Concluding summary

Plate tectonics is an expression of mantle convection and must be understood in terms of chemical and mineralogical compositions, and of related physical properties. Geological, geophysical and geochemical evidence establishes that the convecting upper mantle is lherzolite with approximately 50–60 wt% olivine, 20 wt% orthopyroxene, 10–15 wt% clinopyroxene, and plagioclase, spinel or garnet (at upper mantle *P*, *T* conditions). Chemical composition has $Mg^{\#}$ ~ 90, 3–4 wt% CaO, Al_2O_3 and approximately 0.3–0.5

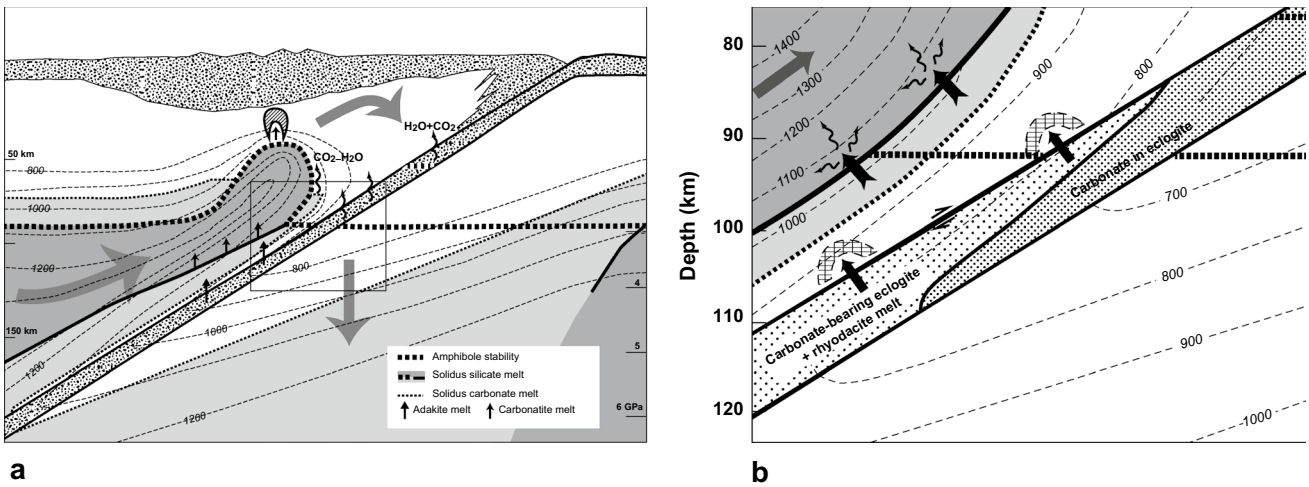

Fig. 18 **a** Diagram illustrating the overlay of temperature contours at a convergent margin with idealised lithologies of subducted slab and overlying mantle wedge. The entire slab/wedge environment is assumed to be relatively oxidised with $H_2O + CO_2$-rich fluids derived from subducted crust and lithosphere. *Stippled pattern* is oceanic crust, fore-arc and magmatic arc; *white areas* are subsolidus lithosphere; *light grey areas* are carbonatite melt in pargasite lherzolite at <~90 km, or in garnet lherzolite at >~90 km; *darker-grey areas* are hydrous silicate melting with lherzolitic to harzburgitic residue. *Rectangular box* is enlarged in **b**. **b** Enlargement of part of **a** to illustrate hydrous dacitic to rhyodacitic melt at >~750 °C in subducted oceanic crust with residual refractory carbonate-bearing eclogite. The melt is depicted as reacting and freezing within overlying peridotite at <950 °C. Dolomitic carbonatite melt is shown as forming at ~950 °C from carbonated peridotite with pargasite (<90 km) or H_2O-rich fluid (>90 km) and migrating through the water-saturated solidus (hydrous silicate melt) in the overlying mantle wedge. The carbonatite melt dissolves in the hydrous silicate melt and upwelling and melt segregation from residual harzburgite to lherzolite yields island arc ankaramite to tholeiite magmas (modified from figure 7.13 in Green and Falloon 1998)

Na_2O, TiO_2. Experimental studies define phase assemblages, including the solidus, as functions of pressure and temperature. Highly incompatible elements, i.e. those with $D^{solid/melt} < 0.1$, may introduce additional minor phases (phlogopite, apatite, sulphides) to the lherzolite mineralogy and consequently have a large effect in lowering solidus temperatures. Most importantly, hydrogen and carbon have major effects on mineralogy and particularly on melting behaviour, and these effects are sensitive to mantle oxidation state. Hydrogen is present as water or hydroxyl solid solution, including limited solubility in olivine, orthopyroxene, clinopyroxene and garnet (NAMs). Water in excess of ~100 ppm in fertile lherzolitic mantle stabilizes the amphibole pargasite to temperatures of 1,050 °C to 1,150 °C at pressures of 1–3 GPa and to depths of ~90 km, the upper mantle solidus is a dehydration melting reaction. However, pargasite is destabilized at 2.8–3.0 GPa by increasing pressure with the result that if water contents exceed ~200 ppm (the maximum water contents in NAMs in fertile lherzolite at ~1,000 °C, 3 GPa), then a water-rich vapour phase is present and the mantle solidus has a large negative dT/dP to intersect the vapour-saturated solidus at 3.0 GPa, 1,025 °C. At higher pressure, the vapour-saturated (water-rich vapour) solidus increases in temperature, approximately parallel to the dry solidus but ~300 °C below it.

Carbon is also present in the upper mantle and introduces complexity in that the mantle oxygen fugacity (fO_2) determines whether oxidised carbon (CO_2, carbonate), elemental carbon (graphite/diamond) or reduced carbon (CH_4) is present. Differing P, T slopes for the C–H–O buffering reactions and the Fe–O reactions, coupled with evidence from magmas and xenoliths from the upper mantle, argue that oxidised carbon is present at shallow depths, graphite/diamond in asthenosphere or deep continental lithosphere, and methane below the asthenosphere. Also carbonation reactions at 1.5–2 GPa between CO_2 fluid and olivine restrict CO_2-rich vapour to the upper lithosphere. Dolomite-bearing lherzolite or dolomitic carbonatite melts occur at >~60 km depth (>1.5–2 GPa) but only in oxidised conditions such as within mature intraplate lithosphere, and in subduction settings.

To a remarkable extent, the presence of very small and variable quantities of hydrogen (water) and carbon (CO_2, carbonate, graphite/diamond and CH_4) is the cause of the thin plate behaviour (plate tectonics) of the modern earth. If a model geotherm for an intraplate setting is overlain on to the phase diagram for fertile lherzolite then it predicts a subsolidus pargasite-bearing lherzolite to ~90 km depth. The geotherm then crosses the solidus for hydrous, carbonate-bearing silicate melt in garnet lherzolite, at temperature ~1,000–1,050 °C. The melt fraction is very small, proportional to the ($H_2O + CO_2$) content, and melt is unable to ascend by porous flow because of reaction to form pargasite. The geotherm remains above the solidus at greater depths as long as water contents exceed ~200 ppm and mantle $fO_2 > IW + 1$ log unit. The lower boundary of the incipient melting layer is the intersection of the geotherm and the lherzolite + (C, H, O) solidus at appropriate fO_2. A very small silicate melt fraction decreases mantle viscosity creating a rheological layering between cool, subsolidus lithosphere overlying asthenosphere with incipient melt, and with underlying subsolidus, high-temperature, convecting mantle (T_p ~ 1,430 °C). The rheological effects of an incipient melting layer at 90–250 km depth offer an explanation for the thin plate behaviour of the Earth (Plate Tectonics). This interpretation may be tested by the ability of lherzolite + (C, H, O), phase relationships in P, T space to match the observed/inferred seismological and electrical conductivity properties of the upper mantle.

The petrology-based model also has significant geochemical implications. The characterisation of the incipient melt in the asthenosphere as carbonated, hydrous, alkali-rich, silica-undersaturated and enriched in highly incompatible elements leads to the prediction of chemical zoning in the asthenosphere. The lower asthenosphere becomes depleted in incompatible elements, acquiring the characteristics of residue after incipient melt extraction at the vapour-saturated (C, H, O vapour) solidus at 4–6 GPa. The incipient melt ponds in the uppermost asthenosphere which becomes enriched in incompatible elements, including CO_2 and H_2O. It is argued that the E-MORB, N-MORB and D-MORB differences in incompatible element and isotopic signatures, and the incompatible-element-enriched intraplate basalts in ocean basins and rifted continental settings, can be interpreted by the model summarised here. Essentially, intraplate and MOR basalt genesis can be understood in terms of mixing or interplay of two components/processes. Component **A** is the major element and compatible trace element abundances determined by the P, T conditions of melting, particularly close to and above the dry solidus of fertile lherzolite. Component **B** is the incompatible-element-enriched, highly silica-undersaturated partial melt in equilibrium with garnet lherzolite at temperatures well below the dry lherzolite solidus. Component **A** reflects the motion and history of the mantle peridotite, and component **B** reflects the additions and depletions of a mobile hydrous, carbonated alkali-rich silicate melt.

Additional complexity is introduced to the melting behaviour of lherzolite by redox reactions accompanying subduction of oxidised crust and mantle into reduced upper mantle and the long-term persistence of old subducted slabs in the convecting mantle. The lherzolite + (C, H, O) phase relations may be applied to convergent margin P, T conditions, with the addition of basaltic, carbonate and continental crust lithologies and their melting behaviour at high pressure and temperature. In subduction settings there is

enhanced importance of H_2O and CO_2 in fluxing melting, and evidence for the dominant roles of melts in transferring major, minor and trace element from subducted slab to overlying mantle wedge peridotite. In the mantle wedge inverted temperature gradients focus melting and production of distinctive primary olivine-rich basaltic magmas. Redox melting (the process in which melting occurs without *P*, *T* change at interfaces between oxidised lithologies with carbonate, oxidised Fe, Cr, Ti, etc. and reduced lithologies with diamond/graphite, reduced Fe, sulphides, and $H_2O + CH_4$ fluids) is important in the subducted slab and in old subducted slab remnants in or below the asthenosphere. The overlay of *P*, *T* models in subduction zones on to phase diagrams predicts locations for hydrous silicate melt extraction and subsolidus carbonate retention in subducted basaltic crust, and in contrast, low-temperature dolomitic carbonatite melt above the slab and below the onset of hydrous melting of peridotite in the high-temperature mantle wedge. Distinctive magma types such as boninites and island arc ankaramites are found only in convergent margin settings and provide evidence for the processes deduced from the phase diagrams. In this setting, the two component nature of primary magmas is again evident. However, the major element and compatible element characteristics include high melt fraction in depleted and refractory peridotite, and higher water contents (from slab-derived fluid) permitting melt segregation well below the dry solidus. Also the added 'incipient melt' components are potentially diverse and may include carbonatite, adakite and water-rich fluid.

The use of high-pressure piston/cylinder apparatus combined with an increasing diversity of microbeam analytical techniques has enabled experimental study of mantle peridotite compositions, their melts and of diverse crustal compositions which may be introduced into the mantle. The synthesis presented here attempts to link the experimental approach with the parallel study of natural peridotites, mantle-derived magmas and mantle xenoliths in magmas.

Acknowledgments This essay on basalts and ultramafic rocks and on the Earth's upper mantle has its beginning in 1,956 in the mapping of an ultramafic complex in northern Tasmania and draws from research carried out from that time to the present, mainly at University of Tasmania and Australian National University. I am grateful for the excellent support of both universities, including continuing 'post-retirement' support from both institutions. As is evident from the text and references, the research summarised is from a team which included excellent technical support (recognising Bill Hibberson and Keith Harris in particular) and successive Ph.D. students, postdoctoral fellows and international visitors. For the theme of this paper, Trevor Falloon, Lynton Jaques, Gerhard Brey, Wayne Taylor, Steve Foley, Margaret Wallace, Kiyoaki Niida, Greg Yaxley, Anja Rosenthal and Istvan Kovacs are particularly acknowledged. Ted Ringwood founded the high-pressure experimental laboratory at ANU and led me from peridotite outcrops to include the upper mantle—his stimulus was central to the theme of this summary. June Pongratz is thanked for preparation of the figures for this paper. I am honoured by the award of the IMA medal and thank Gerhard Brey, Water Maresch and Catherine McCammon for their patience and support in the transformation of 'lecture' to manuscript.

References

Adam J (1990) The geochemistry and experimental petrology of sodic alkaline basalts from Oatlands, Tasmania. J Petrol 31:1201–1223

Asimow PD, Dixon JE, Langmuir CH (2004) A hydrous melting and fractionation model for mid-ocean ridge basalts: application to the Mid-Atlantic ridge near the Azores. Geochem Geophys Geosyst (G-cubed) 5:Q01E16. doi:10.1029/2003GC000568

Berry AJ, Hermann J, O'Neill HSC, Foran GJ (2005) Fingerprinting the water site in mantle olivine. Geology 33:869–872

Brey G, Green DH (1977) Systematic study of liquidus phase relations in olivine melilitite + H_2O + CO_2 at high pressures and petrogenesis of an olivine melilitite magma. Contrib Mineral Petrol 61:141–162

Chalot-Prat F, Falloon TJ, Green DH, Hibberson WO (2010) An experimental study of liquid compositions in equilibrium with plagioclase + spinel lherzolite at low pressures (0.75GPa). J Petrol 51:2349–2376

Chalot-Prat F, Falloon TJ, Green DH, Hibberson WO (2013) Melting of plagioclase + spinel lherzolite at low pressure: an experimental approach to the evolution of basaltic melt during mantle refertilisation at shallow depths. Lithos 172–3:61–80

Cmiral M, FitzGerald JD, Faul UH, Green DH (1998) A close look at dihedral angles and melt geometry in olivine-basalt aggregates: a TEM study. Contrib Mineral Petrol 130:336–345

Conceição RV, Green DH (2000) Behavior of the cotectic curve En–Ol in the system leucite–olivine–quartz under dry conditions to 2.8 GPa. Geochem Geophys Geosyst (G-cubed) 1:2000GL000071

Davies GF (1998) Plates, plumes, mantle convection and mantle evolution. In: Jackson INS (ed) The Earth's mantle: composition, structure and evolution. Cambridge University Press, Cambridge, pp 228–258

Dick HJB (1989) Abyssal peridotites, very slow spreading ridges and ocean ridge magmatism. Geol Soc Spec Pub 42:71–105

Falloon TJ, Green DH (1987) Anhydrous partial melting of MORB pyrolite and other peridotite compositions at 10 kbar and implications for the origin of primitive MORB glasses. Mineral Petrol 37:181–219

Falloon TJ, Green DH (1988) Anhydrous partial melting of peridotite from 8 to 35 kb and the petrogenesis of MORB. J Petrol (Special Lithosphere Issue) 29:379–414

Falloon TJ, Green DH (1989) The solidus of carbonated, fertile peridotite. Earth Planet Sci Lett 94:364–370

Falloon TJ, Green DH (1990) Solidus of carbonated fertile peridotite under fluid-saturated conditions. Geology 18:195–199

Falloon TJ, Green DH, Hatton CJ, Harris KL (1988) Anhydrous partial melting of fertile and depleted peridotite from 2 to 30 kbar and application to basalt petrogenesis. J Petrol 29:257–282

Falloon TJ, Green DH, Danyushevsky LV, Faul UH (1999) Peridotite Melting at 1.0 and 1.5 GPa: an experimental evaluation of techniques using diamond aggregates and mineral mixes for determination of near-solidus melts. J Petrol 40:1343–1375

Falloon TJ, Danyushevsky LV, Green DH (2001) Peridotite melting at 1 GPa: reversal experiments on partial melt compositions produced by peridotite-basalt sandwich experiments. J Petrol 42:2363–2390

Faul UH (2001) Melt retention and segregation at mid-ocean ridges. Earth Planet Sci Lett 176:339–356

Faul UH, Jackson INS (2007) Diffusion creep of dry, melt-free olivine. J Geophys Res 112:B04204. doi:10.1029/2006JB004586(2007

Foley SF (2011) A reappraisal of redox melting in the Earth's mantle as a function of tectonic setting and time. J Petrol 52:1363–1391
Foulger GR (2007) The "plate" model for the genesis of melting anomalies. In: Foulger GR, Jurdy DM (eds) Plates, plumes, and planetary processes, vol 430. Geological Society of America, Boulder, pp 1–28. doi:10.1130/2007.2430(12)
Foulger GR (2010) Plates vs plumes: a geological controversy. Wiley, Oxford, pp 1–328
Frey FA, Green DH, Roy SD (1978) Integrated models of basalt petrogenesis—a study of quartz tholeiites to olivine melilitites from southeastern Australia utilizing geochemical and experimental petrological data. J Petrol 19:463–513
Fumagalli P, Zanchetta S, Poli S (2009) Alkali in phlogopite and amphibole and their effects on phase relations in metasomatized peridotite: a high pressure study. Contrib Mineral Petrol 158:723–737
Garapic G, Faul UH, Brisson E (2013) High resolution imaging of the melt distribution in partially molten upper mantle rocks: evidence for wetted two-grain boundaries. Geochem Geophys Geosyst 14:556–566
Green DH (1971) Composition of basaltic magmas as indicators of conditions of origin: application to oceanic volcanism. Philos Trans R Soc Lond 268:707–725
Green DH (1972) Magmatic activity as the major process in the chemical evolution of the Earth's crust and mantle. Tectonophysics 13:47–71
Green DH (1973a) Conditions of melting of basanite magma from garnet peridotite. Earth Planet Sci Lett 17:456–465
Green DH (1973b) Experimental melting studies on a model upper mantle composition at high pressures under water-saturated and water-undersaturated conditions. Earth Planet Sci Lett 19:37–53
Green DH (1976) Experimental testing of "equilibrium" partial melting of peridotite under water-saturated, high-pressure conditions. Can Mineral 14:255–268
Green DH, Falloon TJ (1998) Pyrolite: A Ringwood concept and its current expression. In: Jackson INS (ed) The Earth's mantle: composition, structure and evolution. Cambridge University Press, Cambridge, pp 311–380
Green DH, Falloon TJ (2005) Primary magmas at mid-ocean ridges, "hotspots", and other intraplate settings: constraints on mantle potential temperature. In: Foulger G, Natland J, Presnall D, Anderson D (eds) Plates, plumes and paradigms, vol 388. Geological Society of America, Boulder, pp 217–247
Green DH, Liebermann RC (1976) Phase equilibria and elastic properties of a pyrolite model for the oceanic upper mantle. Tectonophysics 32:61–92
Green DH, Ringwood AE (1967) The genesis of basaltic magmas. Contr Mineral Petrol 15:103–190
Green DH, Hibberson WO, Jaques AL (1979) Petrogenesis of mid-ocean ridge basalts. In: McElhinny MW (ed) The Earth: its origin, structure and evolution. Academic Press, London, pp 265–290
Green DH, Falloon TJ, Taylor WR (1987), Mantle-derived magmas—roles of variable source peridotite and variable C–H–O fluid compositions. In: Mysen BO (ed) Magmatic processes and physicochemical principles. Geochem Soc Spec Publ No 1, pp 139–154
Green DH, Schmidt M, Hibberson WO (2004) Island-arc ankaramites: primitive melts from fluxed refractory lherzolitic mantle. J Petrol 45:391–403
Green DH, Hibberson WO, Kovacs I, Rosenthal A (2010) Water and its influence on the lithosphere–asthenosphere boundary. Nature 467:448–451
Green DH, Hibberson WO, Kovacs I, Rosenthal A (2011) Addendum to 'Water and its influence on the lithosphere–asthenosphere boundary'. Nature 472:504
Green DH, Hibberson WO, Rosenthal A, Kovacs I, Yaxley GM, Falloon TJ, Brink F (2014) Experimental study of the influence of water on melting and phase assemblages in the upper mantle. J Petrol 55:2067–2096
Grove TL, Chatterjee N, Parman SW, Medard E (2006) The influence of H_2O on mantle wedge melting. Earth Planet Sci Lett 249:74–89
Gupta AK, Green DH (1988) The liquidus surface of the system forsterite–kalsilite–quartz at 28 kb under dry conditions, and in presence of H_2O and CO_2. Mineral Petrol 39:163–174
Gupta AK, Green DH, Taylor WR (1987) The liquidus surface of the system forsterite-nepheline-silica at 28 kb. Am J Sci 287:560–565
Hart SR, Zindler A (1986) In search of a bulk-earth composition. Chem Geol 57:247–267
Hirano N, Takahashi E, Yamamoto J, Abe N, Ingle SP, Kaneoka I, Hirata T, Kimura J, Ishii T, Ogawa Y, Machida S, Suyehiro K (2006) Volcanism in response to plate flexure. Science 313:1426–1428. doi:10.1126/science.1128235
Hirschmann MM (2006) Water, melting, and the deep Earth H_2O cycle. Annu Rev Earth Planet Sci 34:629–653
Jaques AL, Green DH (1980) Anhydrous melting of peridotite at 0-15 kb pressure and the genesis of tholeiitic basalts. Contrib Mineral Petrol 73:287–310
Katz RF, Spiegelman M, Langmuir CH (2003) A new parameterization of hydrous mantle melting. Geochem Geophys Geosyst (G-cubed) 4:1073. doi:10.1029/2002GC000433
Kovacs I, Green DH, Rosenthal A, Hermann J, O'Neill HSC, Hibberson WO, Udvardi B (2012) An experimental study of water in nominally anhydrous minerals in the upper mantle near the water saturated solidus. J Petrol 53:2067–2093
Kushiro I, Syono Y, Akimoto S (1968) Melting of a peridotite nodule at high pressures and high water pressures. J Geophys Res 73:6023–6029
McKenzie D, Bickle MJ (1988) The volume and composition of melt generated by extension of the lithosphere. J Petrol 29:629–679
Mengel K, Green DH (1989) Stability of amphibole and phlogopite in metasomatized peridotite under water-saturated and water-undersaturated conditions. In: Ross J (ed) Kimberlites and related rocks, vol. 1, their composition, occurrence, origin and emplacement. Blackwell, Melbourne, pp 571–581
Millhollen G, Irving AJ, Wyllie PJ (1974) Melting interval of peridotite with 5.7 per cent water to 30 kilobars. J Geol 82:575–587
Morgan WJ (1971) Convection plumes in the lower mantle. Nature 230:42–43
Mysen B, Boettcher AL (1975) Melting of a hydrous mantle: parts I and II. Phase relations of a natural peridotite at high pressures and temperatures with controlled activities of water, carbon dioxide, and hydrogen. J Petrol 16:520–593
Nehru CE, Wyllie PJ (1975) Compositions of glasses from St. Paul's peridotite partially melted at 20 kilobars. J Geol 83:455–471
Niida K, Green DH (1999) Stability and chemical composition of pargasitic amphibole in MORB pyrolite under upper mantle conditions. Contr Mineral Petrol 135:18–40
Niu YL (2004) Bulk-rock major and trace element compositions of abyssal peridotites: implications for mantle melting, melt extraction and post-melting processes beneath ocean ridges. J Petrol 45:2423–2458
Niu YL, O'Hara MJ (2008) Global correlations of ocean ridge basalt chemistry with axial depth: a new perspective. J Petrol 49:633–664
Niu YL, Waggoner DG, Sinton JM, Mahoney JJ (1996) Mantle source heterogeneity and melting processes beneath seafloor spreading centers: the East Pacific Rise, 18–19 S. J Geophys Res 101:27711–27733
O'Reilly SY, Griffin WL (1985) A xenoliths-derived geotherm for south-eastern Australia and its geophysical implications. Tectonophysics 111:41–63
Odling NWA, Green DH, Harte B (1997) The determination of partial melt compositions of peridotitic systems by melt inclusion synthesis. Contrib Mineral Petrol 129:209–221

Ringwood AE (1962) A model for the upper mantle. J Geophys Res 67:857–866

Scott JM, Hodgkinson A, Palin JM, Waight TE, Van der Meer QHA, Cooper AF (2014) Ancient melt depletion overprinted by young carbonatitic metasomatism in the New Zealand lithospheric mantle. Contr Mineral Petrol 167(1). doi:10.1007/s00410-014-0963-0

Taylor WR, Green DH (1987) The petrogenetic role of methane: effect on liquidus phase relations and the solubility mechanism of reduced C–H volatiles. In: Mysen BO (ed) Magmatic processes and physicochemical principles. Geochem Soc Spec Publ No 1, pp 121–138

Taylor WR, Green DH (1988) Measurement of reduced peridotite–C–O–H solidus and implications for redox melting of the mantle. Nature 332:239–352

Taylor WR, Green DH (1989) The role of reduced C–O–H fluids in mantle partial melting. In: Ross J (ed) Kimberlites and related rocks, vol 14. Blackwell, Melbourne, pp 592–602

Till CB, Grove TL, Withers AC (2012) The beginnings of hydrous mantle wedge melting. Contr Mineral Petrol 163:669–688

Tumiati S, Fumagalli P, Tinaboschi C, Poli S (2013) An experimental study on COH-bearing peridotite up to 3.2 GPa and implications for crust–mantle recycling. J Petrol 54:453–479

Wallace ME, Green DH (1988) An experimental determination of primary carbonatite magma composition. Nature 335:343–346

Wallace ME, Green DH (1991) The effect of bulk rock composition on the stability of amphibole in the upper mantle: implications for solidus positions and mantle metasomatism. Mineral Petrol 44:1–19

Wyllie PJ (1978) Mantle fluid compositions buffered in peridotite–CO_2–H_2O by carbonates, amphibole, and phlogopite. J Geol 86:687–713

Wyllie PJ (1979) Magmas and volatile components. Am Mineral 64:469–500

Wyllie PJ, Huang WL, Otto J, Byrnes AP (1983) Carbonation of peridotites and decarbonation of siliceous dolomites represented in the system CaO–MgO–SiO_2–CO_2 to 30 kbar. Tectonophysics 100:359–388

Yaxley GM, Green DH (1996) Experimental reconstruction of sodic dolomitic carbonatite melts from metasomatised lithosphere. Contrib Mineral Petrol 124:359–369

Yaxley GM, Green DH, Kamenetsky V (1998) Carbonatite metasomatism in the southeastern Australian lithosphere. J Petrology 39:1917–1930